haematologica
Journal of the Ferrata Storti Foundation

Protein phosphatase 2A orchestrates hematopoietic fate determination via modulation of lactate metabolism

by Can Liu, Yao Meng, Heng Chen, Siqi Bi, Ye Tian, Zhihua Yin, Guanhua Li, Wutao Chen, Li Wu, You Wang, Nan Shen and Haibo Zhou

Received: August 11, 2025.
Accepted: November 6, 2025.

Citation: Can Liu, Yao Meng, Heng Chen, Siqi Bi, Ye Tian, Zhihua Yin, Guanhua Li, Wutao Chen, Li Wu, You Wang, Nan Shen and Haibo Zhou. Protein phosphatase 2A orchestrates hematopoietic fate determination via modulation of lactate metabolism.
Haematologica. 2025 Nov 13. doi: 10.3324/haematol.2025.288868 [Epub ahead of print]

Protein phosphatase 2A orchestrates hematopoietic fate determination via modulation of lactate metabolism

Can Liu,[1,*] Yao Meng,[1,2,*] Heng Chen,[3,*] Siqi Bi,[1,*] Ye Tian,[1] Zhihua Yin,[4] Guanhua Li,[5] Wutao Chen,[6] Li Wu,[7] You Wang,[6,#] Nan Shen,[1,8,9,10,11,#] Haibo Zhou[1,#]

[1] Shanghai Institute of Rheumatology, Renji Hospital, School of Medicine, Shanghai Jiao Tong University (SJTUSM), 200001 Shanghai, China

[2] Department of Nephrology, Zhongshan Hospital, Fudan University, 200001 Shanghai, China

[3] The Affiliated Wuxi People's Hospital of Nanjing Medical University, Wuxi People's Hospital, Wuxi Medical Center, Nanjing Medical University, 214023 Wuxi, China

[4] Shenzhen Futian Hospital for Rheumatic Diseases, 518040 Shenzhen, China

[5] Department of Nephrology, The First Affiliated Hospital of Zhengzhou University, 450052 Zhengzhou, China

[6] Department of Obstetrics and Gynecology, Renji Hospital, School of Medicine, Shanghai Jiao Tong University (SJTUSM), 200127 Shanghai, China

[7] Tsinghua-Peking Joint Center for Life Sciences, Tsinghua University School of Medicine, Beijing 100084, China

[8] China Australia Centre for Personalized Immunology, Renji Hospital, School of Medicine, Shanghai Jiao Tong University (SJTUSM), 200001 Shanghai, China

[9] State Key Laboratory of Oncogenes and Related Genes, Shanghai Cancer Institute, Renji Hospital, Shanghai Jiao Tong University School of Medicine (SJTUSM), 200032, Shanghai, China

[10] Center for Autoimmune Genomics and Etiology (CAGE), Cincinnati Children's Hospital Medical Center, Cincinnati, Ohio, USA

[11] Department of Pediatrics, University of Cincinnati College of Medicine, Cincinnati, Ohio, USA

[*] These authors contributed equally

Author contributions

HZ, NS, and YW designed the project. CL, YM, HC, and SB performed the experiments. HZ, CL and

YM analyzed the data. CL, GL, YT and SB established the mouse model. HZ, NS, YW, CL, YM, LW and WC prepared the manuscript. CL, YM, HC, and SB contributed equally to this work.

Running head：Lactate contributes to hematopoietic disorders

Corresponding authors

Haibo Zhou: Email: hbzhou1984@163.com; Tel :86-21-63260477;

Nan Shen: Email: nanshensibs@gmail.com; Tel :86-21-63260477;

You Wang: Email: wanghh0163@163.com; Tel :86-21-63260477.

Data-sharing statement

The CUT&Tag and CUT&RUN data generated in this study are available at the Gene Expression Omnibus under accession number GSE248147 and GSE248146, respectively. The RNA profiling data generated in this study are available at the Gene Expression Omnibus with the accession number GSE248148. Other datasets will be made available on request.

Word count: 4528 words. Consisting of 7 figures (Fig. 1-7), 7 supplemental figures and 2 supplemental tables.

Fundings

This study was supported by grants from the National Natural Science Foundation of China (82171767, 82371801, 82572050, 82172918, 82471723, 82101882), the Noncommunicable Chronic Diseases-National Science and Technology Major Project (2024ZD0530601), Youth Project of the Provincial-Ministerial Co-construction for Henan Provincial Medical Science and Technology Research Program (SBGJ202303032), the Shanghai Sailing Program (21YF1424600), the Shanghai Public Health Excellent Discipline Leadership Program (GWVI-11.2-XD15), the Medical-Engineering Joint Funds of Shanghai Jiao Tong University (No. YG2021GD01), and the Clinical Scientific Research Innovation Cultivation Fund of Renji Hospital (No. PYI20-03).

Conflict of interest

The authors declare no competing interests.

Abstract

Abnormal hematopoiesis is inherently linked to metabolic reprogramming. Protein phosphatase 2A (PP2A), a master regulator of hematopoietic homeostasis, has been implicated in multiple hematological disorders. However, the precise mechanisms by which PP2A coordinates metabolic networks to govern hematopoietic fate decisions remain poorly defined. Herein, we identify lactate as a critical mediator of myeloid-biased differentiation triggered by PP2A inactivation. Genetic ablation of *PPP2CA*, the catalytic subunit of PP2A, results in aberrant myeloid proliferation and lymphoid depletion. Transcriptomic profiling reveals that *Ppp2ca* deficiency alters the expression of transcriptional regulators governing hematopoietic lineage commitment and energy metabolism. Metabolomic analyses further demonstrate enhanced lactate metabolism in *Ppp2ca*-deficient hematopoietic progenitors. Importantly, either haploinsufficiency or pharmacological inhibition of lactate dehydrogenase A (LDHA) in vivo effectively reverses the abnormal hematopoiesis induced by *Ppp2ca* deficiency. Mechanistically, *Ppp2ca* deletion directly promotes the transcriptional initiation of glycolytic genes (e.g., *Ldha*) via RNA polymerase II (Pol II). This leads to heightened lactylation of histone deacetylases (HDACs) at specific residues—lysine 412 in HDAC1 and lysine 451 in HDAC2—impairing the assembly of the HDAC1/2/SIN3A co-repressor complex on chromatin, enhancing histone acetylation, and ultimately dysregulating hematopoietic gene expression. Collectively, our work establishes the "PP2A-Lactate-HDAC lactylation" axis as a pivotal regulator of hematopoiesis and identifies LDHA as a promising therapeutic target for PP2A-associated hematological disorders.

Introduction

Protein Phosphatase 2A (PP2A) is a critical serine-threonine phosphatase that is ubiquitously expressed in various cellular subsets.[1, 2] As a versatile phosphatase, PP2A has been demonstrated to regulate more than 30 distinct kinases, such as serine/threonine kinase (AKT), protein kinase C (PKC), p70 S6 kinase, adenosine-3',5'-monophosphate (cAMP) dependent kinases, calcium/calmodulin kinases (CAMK), extracellular signal-regulated kinases (ERK), mitogen-activated protein kinases (MAPK), *etc*.[1, 3, 4] The emerging role of PP2A in the initiation and progression of various cancer and autoimmune disorders has been proposed.[1, 3, 5] Although separate studies have attempted to elucidate the role of PP2A in leukemia, the regulation of hematopoietic homeostasis by PP2A remains to be clarified.[6] Moreover, recent research has revealed that PP2A subunits form a complex with the integrator and exert a broader impact on transcription by directly communicating with RNA polymerase (Pol) II, highlighting the diverse actions of PP2A.[7, 8]

Cellular metabolism is crucial for hematopoietic homeostasis. Dormant hematopoietic stem cells (HSCs) reside within hypoxic niches that exhibit high glycolytic activity and a low yet indispensable rate of fatty acid oxidation (FAO) to maintain quiescence and self-renewal capacity.[9, 10] During the expansion process, HSCs undergo a metabolic shift from quiescence to an activated state. Enhanced mitochondrial oxidative phosphorylation (OXPHOS) is vital for the proliferation of HSCs, supplying precursor molecules for the biosynthesis of amino acids, lipids, and nucleotides.[10-12] Differentiation from multipotent progenitors (MPPs) into myeloid or lymphoid progenitors is characterized by a modest increase in OXPHOS. This is followed by a significant rise in mitochondrial membrane potential and ATP levels when these cells further differentiate into lineage-restricted precursors and mature blood cells.[10-12] As a byproduct of glycolysis, lactate plays a crucial role in both physiological and pathological processes.[13, 14] Post-translational lactylation has been demonstrated to be involved in the tumorigenesis and inflammation.[15-17] While several studies have reported the involvement of lactate in leukemia, its role in the regulation of hematopoiesis and the associated underlying mechanism remains to be elucidated.[18-20]

In this work, we investigated the impact of PP2A deficiency on hematopoiesis through multiple omics approaches, elucidated the intricate crosstalk between lactate metabolism and epigenetic regulation in driving hematopoietic abnormalities, and proposed a novel metabolic target for therapeutic intervention of PP2A-related diseases.

Materials & methods

Mice

The *Ppp2ca-flox* mice (Strain NO. T018350) and *Ldha-flox* mice (Strain NO. T007813) were purchased from GemPharmatech (Nanjing, China). C57BL/6JSmoc-Gt (ROSA)26Sor$^{em1(SA\text{-}FRT\text{-}2xpolyA\text{-}CAG\text{-}FRT\text{-}CreERT2\text{-}Rox\text{-}WPRE\text{-}Rox\text{-}polyA)Smoc}$ mice (Strain NO. NM-KI-200041) were purchased from Shanghai Model Organisms (Shanghai, China). *Ppp2ca-flox* mice were crossed with C57BL/6JSmoc-Gt (ROSA)26Sor$^{em1(SA\text{-}FRT\text{-}2xpolyA\text{-}CAG\text{-}FRT\text{-}CreERT2\text{-}Rox\text{-}WPRE\text{-}Rox\text{-}polyA)Smoc}$ mice to generate $Ert2^{cre}Ppp2ca^{f/f}$ mice. $Ert2^{cre}Ppp2ca^{f/f}$ mice and $Ldha^{f/f}$ were crossed to obtain the $Ert2^{cre}Ppp2ca^{f/f}Ldha^{f/+}$ mice. All mice were bred and housed under specific pathogen-free conditions.

ChIP assay

The ChIP assays were conducted with the Simple ChIP Plus Enzymatic Chromatin IP (Magnetic Beads) Kit (Cell Signaling Technology) according to the protocol. Briefly, cells were cross-linked in 1% formaldehyde for 10 minutes on ice. Chromatin was fragmented through enzyme digestion and sonication, followed by immunoprecipitation of the lysate using an antibody specific to Phospho-Rpb1 CTD (Ser5) (13523, Cell Signaling Technology) or H3K27ac. Subsequently, protein G magnetic beads were added. After washing and elution steps, the cross-links were reversed by heating. The purified DNA fragments were subjected to qPCR analysis, with input DNA (total chromatin) serving as an internal control. The primer sequences are listed in Supplementary Table 2.

ECAR and lactate measurement

Primary cells were seeded into XF96-well plates (Agilent) at a density of $2x10^5$ cells per well in 6 duplicates. Seahorse base media was supplemented with 2mM glutamine. Then, plates were

incubated in a CO_2 free incubator at 37°C for 1 hour, followed by measurement using an XFe96 Analyzer (Agilent). Results were processed with Wave 2.6.0 software. The levels of L-lactate in the cell lysate were quantified using the L-Lactate Assay kit (ab65331, Abcam).

Quantification the enzymatic activities of HDAC

Overexpressed HDAC1-Flag or HDAC2-Flag were immunoprecipitated with an anti-Flag antibody followed by capturing the complex on protein G beads (Cell Signaling Technology). Then, the enzymatic activity of purified HDAC protein was analyzed using the HDAC Activity Assay Kit (colorimetric) (ab1432, Abam).

Tamoxifen induced deletion and pharmaceutical intervention in vivo

Tamoxifen (75 mg/kg) was intraperitoneally injected into mice for 5 consecutive days to remove the *Ppp2ca* gene and/or haploid deletion of *Ldha* gene. The phenotype was analyzed on day 25. For pharmaceutical intervention, sodium oxamate (500 mg/kg) or stiripentol (200 mg/kg) were applied intraperitoneally every other day from day 6 to day 25. For ex-vivo cellular studies, mice were administered intraperitoneal injections of tamoxifen daily for five consecutive days. Five days after the final injection, BM Lin^- or LSK cells were isolated and sorted for subsequent analysis.

Statistics

For comparisons between two independent groups, statistical differences were evaluated using an unpaired two-tailed Student's t-test, with p-values reported in the corresponding figures; a p-value < 0.05 was considered statistically significant. For one-way multi-group analyses (i.e., comparisons involving three or more groups defined by a single independent variable), p-values were calculated via one-way analysis of variance (ANOVA) followed by Tukey's honestly significant difference (HSD) post-hoc test to correct for multiple comparisons. For two-way multi-group analyses (i.e., comparisons involving groups defined by two independent variables), p-values were determined using two-way analysis of variance (ANOVA) with subsequent Bonferroni post-hoc test to account for multiple pairwise comparisons. Statistical analysis was performed using the Graph Prism 7.0 software (GraphPad Software Inc.).

Ethics approval statement

All animal experiments were ethically approved by the Animal Care Committee of Renji Hospital.

Results

PP2A modulates hematopoietic lineage commitment

PP2A phosphatase consists of a scaffolding subunit A, a regulatory subunit B and a catalytic subunit C.[7] To investigate the consequences of PP2A deficiency, we employed genetic ablation of the *Ppp2ca* gene, which encodes the catalytic subunit of PP2A. Since mice with hematopoietic deletion of *Ppp2ca* are lethal, we utilized the tamoxifen-induced *Ppp2ca* knockout (KO) mice to investigate the contribution of PPP2CA in hematopoietic lineage commitment. The efficiency of *Ppp2ca* deletion has been confirmed (*Supplementary Figure 1A*). *Ppp2ca* KO mice displayed splenomegaly, thymic atrophy, and a significant increase in splenocyte counts (Figure 1A and B; *Supplementary Figure 1B*). A substantial reduction was found in the percentage of splenic lymphoid cells, including B cells, $CD4^+$ T cells and $CD8^+$ T cells, in *Ppp2ca* KO mice (Figure 1C; *Supplementary Figure 1C*). On the contrary, the percentage of splenic myeloid cells, including granulocytes, monocytes and macrophages was found to be increased (Figure 1D; *Supplementary Figure 1C*). No significant difference was found in the proportion of splenic DC subsets (Figure 1E; *Supplementary Figure 1C*). In line with this, a significant reduction in the number of splenic B cells and $CD4^+$ T cells and an elevation in the number of splenic granulocytes, monocytes, macrophages, pDCs and cDC2 were observed in KO mice (Figure 1F-H). There was minimal difference in the number of total BM cells (Figure 1I). Similar to the splenic phenotype, the proportion of B cells was significantly reduced while those of granulocytes and monocytes were found to be markedly increased in the BM of *Ppp2ca* KO mice (Figure 1J-L; *Supplementary Figure 1C*). Although the number of BM monocytes was statistically similar between *Ppp2ca* WT and KO mice, the number of BM B cells was reduced and the number of BM granulocytes was increased in *Ppp2ca* KO mice (Figure 1M-O). When we further examined the composition of hematopoietic progenitors in the BM, we found no significant difference between *Ppp2ca* WT and KO mice in the number of lineage negative (Lin^-) cells and the proportion of myeloid progenitors, including granulocyte-monocyte progenitor (GMP), common myeloid progenitor (CMP) and

megakaryocyte-erythroid progenitor (MEP) (Figure 1P and Q; *Supplementary Figure 1C*). In contrast, both the percentage and the absolute number of common lymphoid progenitor (CLP) were decreased following *Ppp2ca* deletion (Figure 1R and S). Further tracing back to the HSC stage, there were no statistical differences observed in $Lin^{-}Sca\text{-}1^{+}c\text{-}Kit^{+}$ (LSK) cells and their subsets, including long-term HSC (LT-HSC), short-term HSC (ST-HSC), MMP2, MMP3, and MMP4 (*Supplementary Figure 1D and 2A and B*). Therefore, we focused on the regulatory role of PPP2CA in the myeloid and lymphoid lineage commitment downstream of LSK.

Ppp2ca deficiency leads to dysregulated expression of genes involved in hematopoietic and metabolic pathways

To elucidate the underlying mechanism of PP2A in regulating hematopoiesis, we investigated the transcriptional changes in LSK cells following *Ppp2ca* deletion. Compared with WT mice, the top enriched pathway of down-regulated genes in LSK cells from *Ppp2ca* KO mice was the hematopoietic cell lineage pathway (Figure 2A). More precisely, the expression of lineage-related genes associated with HSC, erythroid-megakaryoid and lymphoid lineage was reduced in LSK cells from *Ppp2ca* KO mice (Figure 2B). To be specific, *Flt3*, *Flt3l*, *Kit, Il6* and *Il6ra* are critical for the stemness maintenance of HSC. *Il7* and *Il7r*, as well as *Epor*, are respectively critical for the development of lymphoid and erythroid cells (Figure 2B) By contrast, the expression of myeloid-determining genes, including *Cebpα*, *Cebpβ*, *CebpƐ*, *Csf2ra*, *Csf2rb* and *Csf2rb2*, was increased in LSK cells from *Ppp2ca* KO mice (Figure 2B).

The majority of upregulated genes in *Ppp2ca*-deficient LSK cells were enriched in various metabolic pathways, such as amino acid biosynthesis, carbon metabolism, the pentose phosphate pathway (PPP), glycolysis, *etc*. (Figure 2C). Of note, there was a significant increase in the expression of genes associated with glycolysis and the mitochondrial electron transport chain (Figure 2D). Gene set enrichment analysis (GSEA) further demonstrated that the potential of T cell differentiation, and B cell differentiation was impaired, while pathways related to the myeloid cell development, glycolysis, OXPHOS, MTORC1 signaling, Myc targets and Myeloid CEBPA network were enhanced in LSK cells following *Ppp2ca* deletion. (Figure 2E-G).

To further characterize the global transcriptomic divergence between WT and KO LSK cells, we conducted Principal Component Analysis (PCA). As an unbiased analytical approach, PCA effectively validated the reliability of transcriptomic differences between the two groups, ensuring that the observed variations were driven by the genetic background rather than technical artifacts (*Supplementary Figure 2C*). Moreover, unbiased identification of differentially expressed genes (DEGs) revealed additional candidate regulators, such as *Gimap6*, *Six1*, and *Gas6*, which are potentially implicated in mediating the hematopoietic regulatory network disrupted by *Ppp2ca* deficiency (*Supplementary Figure 2D*). Additionally, we confirmed that the protein levels of key glycolytic enzymes—including HK2, PFKP, PKM2, and LDHA—were elevated in KO LSK cells (*Supplementary Figure 2E*).

Ppp2ca deficiency results in metabolic abnormalities

Considering the extensive regulation of metabolic pathways by *Ppp2ca*, we subsequently investigated the impact of *Ppp2ca* deficiency on LSK cell metabolism and found an increase in metabolites associated with energy production and material synthesis, including glycolysis, PPP, fatty acid oxidation (FAO), the tricarboxylic acid cycle (TCA), *etc.* (Figure 3A and B). Seahorse analysis revealed a significant increase in glycolytic activity in *Ppp2ca* deficient LSK cells, as evidenced by elevated extracellular acidification rate (ECAR) (Figure 3C). The accumulation of lactate and an increased ratio of NAD^+/NADH were observed following *Ppp2ca* deletion (Figure 3D and E). It was consistent with the RNA profiling data that genes encoding key glycolytic enzymes were upregulated in *Ppp2ca*-deficient LSK cells, such as *Hk2*, *Pfkp*, *Pkm*, *Ldha*, et al (Figure 2D and 3A). Interestingly, the expression of *Tigar* and *G6pdx*, two enzymes previously implicated in the PPP-dependent development of B cell malignancies, was also found to be increased after *Ppp2ca* deletion (Figure 3A).[21] Furthermore, increased levels of intracellular reactive oxygen species (ROS)—encompassing both cytosolic and mitochondrial fractions—were detected in LSK cells with *Ppp2ca* deficiency (Figure 3F).

Ppp2ca keeps the transcription of glycolytic genes in check

We next explored the mechanism by which PPP2CA regulates metabolism. Recent studies have unveiled that PPP2CA forms a complex with integrator and exerts a transcriptional inhibitory

effect by directly communicating with RNA polymerase (Pol) II.[7] In order to verify the involvement of this novel paradigm in hematopoiesis, we detected the chromatin binding of PPP2CA by using the cleavage under targets and tagmentation (CUT&Tag) technology. Consistent with the previous report,[7] a majority of PPP2CA binding sites (63.98%) were found to be located within the promoter region, primarily in the core promoter regions (≦1kb) (*Supplementary Figure 3A and B*). Global analysis of associated genes revealed that the metabolic pathway was significantly enriched and ranked as the top pathway (*Supplementary Figure 3C*). Upon conducting a more in-depth analysis of metabolic genes, we discovered that these genes were enriched in the biosynthesis of amino acids, central carbon metabolism in cancer, glycolysis, *Hif-1* signaling, and the PPP pathways (Figure 4A). Specifically, the promoter loci of key glycolytic enzymes (*Hk2*, *Pfkp*, *Pkm*, *Ldha, etc.*) could be occupied by PPP2CA (Figure 4B). In contrast, PPP2CA failed to bind to the promoter regions of the hematopoietic lineage-related genes (*Supplementary Figure 3D*). Furthermore, the occupancy of phosphorylated Ser^5 within the Pol II C-terminal domain (CTD), a well-established indicator of transcription initiation, was validated to be increased at the promoters of metabolic genes rather than at those of lineage-associated genes (Figure 4C). Collectively, *Ppp2ca* deficiency directly promotes the transcriptional initiation of glycolytic genes in LSK cells.

Haploid deletion of the *Ldha* gene alleviates the abnormal hematopoiesis in *Ppp2ca*-deficient mice

The metabolomics analysis revealed a remarkable accumulation of lactate in *Ppp2ca*-deficient LSK cells. Lactate plays a pivotal role in coordinating diverse physiological and pathological processes, either through direct action or epigenetic lactylation.[13] To investigate the contribution of lactate to the hematopoietic abnormalities in *Ppp2ca*-deficient mice, we evaluated the impact of the *Ldha* gene, which encodes the A subunit of lactate dehydrogenase enzyme responsible for pyruvate to lactate conversion, on this process. The elevation of lactate levels was observed following *Ppp2ca* deletion (Figure 5A). In contrast, haploid deletion of *Ldha* restored the lactate levels in *Ppp2ca*-deficient hematopoietic progenitor cells to normalcy (Figure 5A). The deletion of *Ppp2ca* resulted in a substantial decline in the populations of BM B cells, as well as splenic B and T cell subsets (Figure 5B and C). Concomitantly, there was an increase in the proportion of

granulocytes and monocytes within the BM and spleen, along with an elevation in the proportion of macrophages in the spleen (Figure 5B and C). Conversely, the composition of DC subsets remained largely unchanged, except for a slight decrease in splenic pDCs in mice with haploid deletion of *Ldha* (Figure 5C). Meanwhile, it was discovered that the proportion of CLP decreased (Figure 5D). Significantly, haploid deletion of the *Ldha* gene was found to be sufficient to alleviate the defects caused by *Ppp2ca* deficiency, thereby restoring the normal proportions of B cells, granulocytes, monocytes, and CLP in the BM, as well as the those of B cells, T cells, granulocytes, monocytes and macrophages in the spleen (Figure 5B-D). By the way, the composition of other progenitors, including CMP, GMP and MEP, was unaffected upon *Ppp2ca* deletion together with or without *Ldha* haploid insufficiency (Figure 5D). Therefore, *Ldha* is the key enzyme mediating the regulation of *Ppp2ca* on hematopoietic differentiation.

Pharmacological interventions targeting lactate metabolism reverse the hematopoietic defects caused by *Ppp2ca* deficiency

Since the genetic intervention targeting elevated lactate reversed the hematopoietic disorders caused by *Ppp2ca* deletion, we further investigated the in vivo effects of two distinct *Ldha* inhibitors, oxamate and stiripentol, on the treatment of *Ppp2ca*-deficient mice (*Supplementary Figure 4A*).[20, 22, 23] The application of stiripentol alleviated the phenotypic defects by restoring the proportion of B cells, granulocytes, and monocytes to normal levels (*Supplementary Figure 4B-D, G and H*). In contrast, administration of sodium oxamate exhibited relatively modest therapeutic efficacy, failing to fully restore the normal differentiation of granulocytes and monocytes within the spleen (*Supplementary Figure 4G and H*). Although neither oxamate nor stiripentol could completely mitigate the decline in T cell subsets, their application resulted in a partial recovery of the T cell proportion (*Supplementary Figure 4E and F*). Besides, when detecting the progenitors, we found that the decrease in CLP was reversed by stiripentol (*Supplementary Figure 4I*). Furthermore, no significant difference was observed in the proportion of myeloid progenitors among the groups (*Supplementary Figure 4J*). Therefore, the excessive accumulation of lactate represents the primary pathogenic mechanism underlying hematopoietic abnormalities in *Ppp2ca*-deficient mice.

Increased lactylation of HDAC1 and HDAC2 upon deletion of *Ppp2ca*

To elucidate the underlying mechanism of lactate driven hematopoietic abnormalities, we conducted comprehensive research utilizing lactyl-modification omics. Mass spectrometry (MS) analysis revealed that upregulated lactylation was observed in 89 out of 90 differentially lactyl-modified sites (Figure 6A). These sites were distributed across 67 proteins, among which 10 proteins had been proven to be associated with hematopoiesis (Figure 6B). No significant change in histone (H) lactylation was observed upon re-confirmation with immunoblotting screening (*Supplementary Figure 5*). Of note, both HDAC1 and HDAC2 were particularly critical. The lactylated lysine residues (K), including the 412th K (K412) in HDAC1 and the 451st K (K451) in HDAC2, along with their respective adjacent peptides, were found to be conserved across human and mouse (Figure 6C, D). Immunoblotting analyses validated the upregulated lactylation of HDAC1 and HDAC2 in *Ppp2ca* deficient LSK (Figure 6E). When lactate metabolism was blocked by the application of oxamate, a significant reduction in the levels of Klac in LSK cells was observed (Figure 6E). Concurrently, the global acetylation of K (Kac) in *Ppp2ca* deficient LSK was found to be elevated (Figure 6F). These findings strongly suggest that the augmented lactyl-modification may potentially attenuate the deacetylation function of HDACs.

Enhanced lactylation of HDACs contributes to the excessive expression of myeloid determining genes following *Ppp2ca* deletion

To assess the influence of lactylation on the enzymatic activities of HDAC1 and HDAC2, the K412 in HDAC1 and the K451 in HDAC2 were genetically mutated to arginine (HDAC1 R412 and HDAC2 R451). This approach, which involves substituting K with R at specific residues, is a widely acknowledged and validated experimental strategy for investigating the functional roles of lactylated sites within proteins.[15,24-26] Furthermore, we ascertained that no additional modifications occurred at these two specific sites. Remarkably, the replacement of K by R resulted in a substantial decline in the lactylation levels of HDAC1 and HDAC2 (Figure 6G). When conducting in vitro analysis of enzyme activity, we found that these mutations did not compromise the deacetylation capabilities of HDAC1 and HDAC2 (Figure 7A). It has been reported that the K412 residue in HDAC1 is adjacent to the “IACEE” domain, which is required for its interaction with pocket proteins. And, the K451 residue in HDAC2 is situated within the coiled coil

domain (CCD), that mediates the binding of HDAC2 to other proteins, including the subunits of co-repressors (Figure 7B).[27, 28] Therefore, we postulated that the upregulated lactyl-modification might impede the functional assembly of HDAC repressors on chromatin, and consequently led to excessive histone acetylation.

Class I HDACs are capable of assembling into four distinct protein complexes, namely SIN3,[29] NuRD,[30] CoREST,[31] and MiDac,[32] exerting a role of histone deacetylation. Among them, the SIN3 complex has been identified as indispensable for hematopoiesis.[33] It has been reported that genetic ablation of *Sin3a,* the core subunit of SIN3 complex, results in hematopoietic disorders that phenotypically resemble those in HDAC1 and HDAC2 double deficient (DKO) mice.[33] More importantly, through an integrative structural analysis of the SIN3A/HDAC complex utilizing Halo affinity capture, chemical crosslinking, and high-resolution mass spectrometry (XL-MS), it was revealed that K412 resides in a region where HDAC1 directly interacts with other subunits, including NGDN, SIN3A, and SAP30L. Additionally, K451 is positioned within a domain responsible for the self-interaction of HDAC2 in the SIN3A/HDAC co-repressor.[34] In light of these findings, we devised co-immunoprecipitation assays to assess the influence of lactylation at these two sites on the interaction between HDACs and SIN3A. Our results indicated that the K412R substitution strengthened the interaction of HDAC1 with endogenous HDAC2 and SIN3A (Figure 7C). Analogously, the K451R mutation promoted the binding of HDAC2 with endogenous HDAC1 and SIN3A (Figure 7C). Collectively, these data suggest that site-specific lactylation of HDACs weakens the assembly of the SIN3A/HDAC complex.

To investigate the consequences of hyper-lactylated HDAC1 and HDAC2, we firstly assessed the alteration of histone (H) 3 K27 acetylation (H3K27ac), a well-characterized chromatin marker of active promoters and enhancers,[35, 36] in *Ppp2ca* deficient LSK. Upon deletion of *Ppp2ca*, a global elevation in H3K27ac levels was detected (*Supplementary Figure 6A*). Specifically, the findings demonstrated an increased occupancy of H3K27ac at the promoters of genes crucial for myeloid determination, including *Cebpα*, *Cebpβ*, *Cebpε*, *Csf2ra*, *Csf2rb* and *Csf2rb2* (*Supplementary Figure 6B*). These hyper-acetylated sites were notably enriched in mTOR, G1/S transition and AKT pathways (*Supplementary Figure 6C*). Consistently, genes upregulated in *Ppp2ca* deficient LSK

also exhibited heightened H3K27 acetylation (*Supplementary Figure 6D*). Moreover, the augmented acetylation of H3K27 at the promoters of *Cebpα*, *Cebpℰ*, *Csf2ra*, *Csf2rb* and *Csf2rb2* was confirmed by CHIP-qRT-PCR (Figure 7D). Finally, the application of oxamate effectively suppressed the excessive acetylation of H3K27 (Figure 7E). Furthermore, haploid deletion of *Ldha* also alleviated the increased H3K27ac caused by *Ppp2ca* deficiency (Figure 7F). Therefore, these results suggest that lactate mediates the regulatory effect of PPP2CA on H3K27 acetylation.

Discussion

In this study, we utilized multi-omic approaches to elucidate the metabolic and epigenetic alterations consequent to *Ppp2ca* deletion. The deficiency of *Ppp2ca* promoted RNA polymerase II-mediated initiation of glycolytic genes and lactate accumulation. Subsequently, the elevated lactate metabolism facilitated the lactylation of HDACs. This process impeded the assembly of the HDAC/SIN3A complex, thereby increasing the levels of H3K27 acetylation and upregulating the expression of myeloid-determination genes. As a result, it induced a reduction in lymphoid cells and an expansion of myeloid cells (*Supplementary Figure 7*).

Previous studies reported that PP2A redirected glucose utilization towards the PPP metabolism in B cells, promoting the survival of B cells and the progression of B cell tumors.[21] The balance maintained by the activity of PP2A and B-cell transcriptional factors (TFs) PAX5 and IKZF1 plays a gatekeeper role in the B cell malignancies.[21] However, our findings indicate that PP2A exerts a profound impact on the maintenance of hematopoietic homeostasis and is indispensable for the development of both B and T cells. *Ppp2ca* KO mice exhibit a reduced proportion of CLP and terminally differentiated lymphocytes, while lactate blockade can restore normal hematopoiesis in *Ppp2ca*-deficient mice. Therefore, PP2A and downstream lactate metabolism play important roles in early stage of lineage determination, far beyond their influence on terminally differentiated B cells.

The classical model for PP2A regulation generally focuses on its capacity to dephosphorylate a wide range of proteins, especially the molecules in PI3K-AKT-mTOR pathway.[37-40] However, our findings reveal that *Ppp2ca* deficiency directly facilitated the RNA transcriptional initiation of

various metabolic genes mediated by Pol II, including genes significantly enriched in the glycolytic pathway. This result highlights that *Ppp2ca* can serve as a critical regulatory gene that directly orchestrates metabolism. Subsequently, the "Warburg effect" and the accumulation of lactate were observed in *Ppp2ca*-deficient LSK cells, leading to the elevated lactylation of HDAC1 and HDAC2. Thus, our work establishes a novel "PP2A-LDHA-HDAC" axis in the regulation of hematopoiesis.

Both HDAC1 and HDAC2 are required for the maintenance of hematopoietic homeostasis in a functional complementary way.[33, 41, 42] Single deletion of *Hdac1* or *Hdac2* had little effect on hematopoiesis. Simultaneous loss of *Hdac1* and *Hdac2* (*Hdac1*$^{\Delta/\Delta}$*Hdac2*$^{\Delta/\Delta}$) significantly impaired the reconstituting abilities of hematopoietic stem cells.[33, 42] Genetic deletion of *Sin3a* exhibited a comparable phenotype to *Hdac1*$^{\Delta/\Delta}$*Hdac2*$^{\Delta/\Delta}$ mice.[33] Conditional KO of *Sin3a* further demonstrated that *Sin3a* was essential for T- and B-lymphocyte development.[33] Likewise, we found that BM inactivation of *Ppp2ca* led to a decline in the expression of genes for hematopoietic stem cell maintenance. And *Ppp2ca* was revealed indispensable for the differentiation of T cell and B cells. The phenotypic resemblance among *Ppp2ca* KO mice, *Sin3a* KO mice and *Hdac1/2* DKO mice strongly corroborates our conclusion that the impaired formation of HDAC/SIN3A complex ultimately mediated the epigenetic remodeling and hematopoietic dysfunction in *Ppp2ca* deficient HSCs. In addition, the direct lactylation of histones has garnered substantial research interest in recent years[16]. Nevertheless, no significant disparities in histone lactylation were detected between the WT and KO Lin$^-$ cells, regardless of whether modification proteomics or immunoblotting assays were used.

C/EBPα is mainly involved in cell fate decisions towards myeloid differentiation. It acts as a pioneer TF in cooperation with other TFs to prime the myeloid gene expression program as early as LT-HSC.[43, 44] C/EBPα, in collaboration with PU.1 or C/EBPβ, redirects the lymphoid progenitors towards myeloid progenitors to eventually differentiate into monocytes/granulocytes.[44] C/EBPε, acting downstream of C/EBPα, is required for terminal granulopoiesis.[45, 46] The GM-CSF pathway is involved in the generation of granulocytes, macrophages, and dendritic cells from hematopoietic progenitors. Increased expression of GM-CSF receptors on hematopoietic

progenitor cells during inflammation promotes a striking increase in myelopoiesis at the earliest hematopoietic stages.[47, 48] Therefore, the upregulated expression of *Cebpα*, *Cebpℰ*, *Csf2ra*, *Csf2rb* and *Csf2rb2* in *Ppp2ca*-deficient LSK cells due to enhanced acetylation of H3K27 led to aberrant myelopoiesis. Furthermore, as it has been well-documented that *C/EBPα* deficiency can result in an augmented quantity and enhanced repopulating capacity of HSCs,[43] the upregulated expression of *Cebpα* may potentially play a role in the downregulation of HSC-related genes within the *Ppp2ca*-deficient LSK.

Notably, the alteration in the proportion of DCs is less prominent than that observed in other immune cell subsets in KO mice. There may be two reasons for these results. On the one hand, accumulating studies have confirmed that DCs originate from hematopoietic progenitors that are distinct from lymphoid and myeloid progenitors.[49-51] Thus, *Ppp2ca* exerts differential effects on the differentiation potential of distinct progenitor subsets. On the other hand, it has been reported that *Cebpα*—whose expression is elevated in the HSCs of KO mice (Fig. 2B)—is essential for the differentiation of stem/progenitor cells into common DC progenitors (CDPs), but is dispensable for the subsequent transition of CDPs to mature DCs.[52] Thus, the upregulated *Cebpα* expression in KO HSCs may provide a mechanistic explanation for the mild increase in the numbers of cDCs and pDCs observed in our study (Fig. 1H). Moreover, high levels of *Cebpα* can drive lymphoid-to-myeloid lineage reprogramming of hematopoietic progenitors.[53] This lineage-shifting effect of *Cebpα* overexpression may account for the more profound changes in the populations of T cells, B cells, monocytes, and granulocytes—starkly contrasting with the mild alterations in DC subsets.

In addition to *Ldha*, several other genes—including *Gimap6*, *Six1*, and *Gas6*—are also implicated in regulating the abnormal phenotypes associated with *Ppp2ca* deficiency. *Gimap6* is essential for maintaining T cell survival and homeostasis.[54] The marked downregulation of *Gimap6* in KO model thus likely contributes to the reduced proportion of T cells, which aligns with the observed immunophenotypic abnormalities. *Six1* has been shown to promote the maintenance of myeloid leukemia stem cells and enhance myeloid proliferation.[55] Consequently, the elevated expression of *Six1* in KO mice may drive the abnormal expansion of myeloid cells. *Gas6* is well characterized

as a potent growth factor that supports the robust expansion of HSC.[56] The reduced *Gas6* expression in KO mice is consistent with the diminished expression of HSC lineage-specific genes in *Ppp2ca*-deficient LSK cells.

As the most abundant phosphatase with broad effect, PP2A has emerged as a pivotal therapeutic target for diverse tumors, including leukemia.[57] Moreover, *Ppp2ca* has been identified as a lupus susceptibility gene and the PP2A activator fingolimod/FTY720 has been approved by FDA for the treatment of multiple sclerosis.[58, 59] In this work, pharmacological inhibition of lactate significantly ameliorated the abnormalities resulting from PP2A dysfunction. Therefore, our research proposes lactate blockade as a potential novel treatment for a broad range of PP2A-associated disorders.

References

1. Perrotti D, Neviani P. Protein phosphatase 2A: a target for anticancer therapy. Lancet Oncol. 2013;14(6):e229-238.

2. Junttila MR, Puustinen P, Niemelä M, et al. CIP2A Inhibits PP2A in Human Malignancies. Cell. 2007;130(1):51-62.

3. Seshacharyulu P, Pandey P, Datta K, Batra SK. Phosphatase: PP2A structural importance, regulation and its aberrant expression in cancer. Cancer Lett. 2013;335(1):9-18.

4. Ciccone M, Calin GA, Perrotti D. From the Biology of PP2A to the PADs for Therapy of Hematologic Malignancies. Front Oncol. 2015;5:21.

5. Sharabi A, Kasper IR, Tsokos GC. The serine/threonine protein phosphatase 2A controls autoimmunity. Clin Immunol. 2018;186:38-42.

6. Goswami S, Mani R, Nunes J, et al. PP2A is a therapeutically targetable driver of cell fate decisions via a c-Myc/p21 axis in human and murine acute myeloid leukemia. Blood. 2022;139(9):1340-1358.

7. Zheng H, Qi Y, Hu S, et al. Identification of Integrator-PP2A complex (INTAC), an RNA polymerase II phosphatase. Science. 2020;370(6520):eabb5872.

8. Vervoort SJ, Welsh SA, Devlin JR, et al. The PP2A-Integrator-CDK9 axis fine-tunes transcription and can be targeted therapeutically in cancer. Cell. 2021;184(12):3143-3162.e32.

9. Jones CL, Inguva A, Jordan CT. Targeting Energy Metabolism in Cancer Stem Cells: Progress and Challenges in Leukemia and Solid Tumors. Cell Stem Cell. 2021;28(3):378-393.

10. Nakamura-Ishizu A, Ito K, Suda T. Hematopoietic Stem Cell Metabolism during Development and Aging. Dev Cell. 2020;54(2):239-255.

11. Rattigan KM, Zarou MM, Helgason GV. Metabolism in stem cell-driven leukemia: parallels between hematopoiesis and immunity. Blood. 2023; 41(21):2553-2565.

12. Filippi MD, Ghaffari S. Mitochondria in the maintenance of hematopoietic stem cells: new perspectives and opportunities. Blood. 2019;133(18):1943-1952.

13. Li X, Yang Y, Zhang B, et al. Lactate metabolism in human health and disease. Signal Transduct Target Ther. 2022;7(1):305.

14. Brooks GA. The Science and Translation of Lactate Shuttle Theory. Cell Metab.

2018;27(4):757-785.

15. Zhang D, Tang Z, Huang H, et al. Metabolic regulation of gene expression by histone lactylation. Nature. 2019;574(7779):575-580.

16. Certo M, Tsai C-H, Pucino V, Ho P-C, Mauro C. Lactate modulation of immune responses in inflammatory versus tumour microenvironments. Nat Rev Immunol. 2020;21(3):151-161.

17. Yang Z, Yan C, Ma J, et al. Lactylome analysis suggests lactylation-dependent mechanisms of metabolic adaptation in hepatocellular carcinoma. Nat Metab. 2023;5(1):61-79.

18. Ordonez-Moreno L-A, Haddad M, Chakrabarti P, et al. Lactate-a new player in G-CSF-induced mobilization of hematopoietic stem/progenitor cells. Leukemia. 2023;37(8):1757-1761.

19. Wang Y-H, Israelsen WJ, Lee D, et al. Cell-State-Specific Metabolic Dependency in Hematopoiesis and Leukemogenesis. Cell. 2014;158(6):1309-1323.

20. Chen Q, Xin M, Wang L, et al. Inhibition of LDHA to induce eEF2 release enhances thrombocytopoiesis. Blood. 2022;139(19):2958-2971.

21. Xiao G, Chan LN, Klemm L, et al. B-Cell-Specific Diversion of Glucose Carbon Utilization Reveals a Unique Vulnerability in B Cell Malignancies. Cell. 2018;173(2):470-484.e18.

22. Rho H, Terry AR, Chronis C, Hay N. Hexokinase 2-mediated gene expression via histone lactylation is required for hepatic stellate cell activation and liver fibrosis. Cell Metab. 2023;35(8):1406-1423.e8.

23. Sada N, Lee S, Katsu T, Otsuki T, Inoue T. Epilepsy treatment. Targeting LDH enzymes with a stiripentol analog to treat epilepsy. Science. 2015;347(6228):1362-1367.

24. Chen Y, Wu J, Zhai L, et al. Metabolic regulation of homologous recombination repair by MRE11 lactylation. Cell. 2024;187(2):294-311.e21.

25. Sun L, Zhang Y, Yang B, et al. Lactylation of METTL16 promotes cuproptosis via m(6)A-modification on FDX1 mRNA in gastric cancer. Nat Commun. 2023;14(1):6523.

26. Xiong J, He J, Zhu J, et al. Lactylation-driven METTL3-mediated RNA m(6)A modification promotes immunosuppression of tumor-infiltrating myeloid cells. Mol Cell. 2022;82(9):1660-1677.e10.

27. Brunmeir R, Lagger S, Seiser C. Histone deacetylase HDAC1/HDAC2-controlled embryonic development and cell differentiation. Int J Dev Biol. 2009;53(2-3):275-289.

28. Ma P, Schultz RM. HDAC1 and HDAC2 in mouse oocytes and preimplantation embryos: Specificity versus compensation. Cell Death Differ. 2016;23(7):1119-1127.

29. Hassig CA, Fleischer TC, Billin AN, Schreiber SL, Ayer DE. Histone deacetylase activity is required

for full transcriptional repression by mSin3A. Cell. 1997;89(3):341-347.

30. Xue Y, Wong J, Moreno GT, Young MK, Côté J, Wang W. NURD, a novel complex with both ATP-dependent chromatin-remodeling and histone deacetylase activities. Mol Cell. 1998;2(6):851-861.

31. You A, Tong JK, Grozinger CM, Schreiber SL. CoREST is an integral component of the CoREST-human histone deacetylase complex. Proc Natl Acad Sci U S A. 2001;98(4):1454-1458.

32. Bantscheff M, Hopf C, Savitski MM, et al. Chemoproteomics profiling of HDAC inhibitors reveals selective targeting of HDAC complexes. Nat Biotechnol. 2011;29(3):255-265.

33. Heideman MR, Lancini C, Proost N, Yanover E, Jacobs H, Dannenberg JH. Sin3a-associated Hdac1 and Hdac2 are essential for hematopoietic stem cell homeostasis and contribute differentially to hematopoiesis. Haematologica. 2014;99(8):1292-1303.

34. Banks CAS, Zhang Y, Miah S, et al. Integrative Modeling of a Sin3/HDAC Complex Sub-structure. Cell Rep. 2020;31(2):107516.

35. Wang M, Chen Z, Zhang Y. CBP/p300 and HDAC activities regulate H3K27 acetylation dynamics and zygotic genome activation in mouse preimplantation embryos. EMBO J. 2022;41(22):e112012.

36. Lai TH, Ozer HG, Gasparini P, et al. HDAC1 regulates the chromatin landscape to control transcriptional dependencies in chronic lymphocytic leukemia. Blood Adv. 2023;7(12):2897-2911.

37. Janghorban M, Farrell AS, Allen-Petersen BL, et al. Targeting c-MYC by antagonizing PP2A inhibitors in breast cancer. Proc Natl Acad Sci U S A. 2014;111(25):9157-9162.

38. Pippa R, Odero MD. The Role of MYC and PP2A in the Initiation and Progression of Myeloid Leukemias. Cells. 2020;9(3):544.

39. Allen-Petersen BL, Risom T, Feng Z, et al. Activation of PP2A and Inhibition of mTOR Synergistically Reduce MYC Signaling and Decrease Tumor Growth in Pancreatic Ductal Adenocarcinoma. Cancer Res. 2019;79(1):209-219.

40. Farrington CC, Yuan E, Mazhar S, et al. Protein phosphatase 2A activation as a therapeutic strategy for managing MYC-driven cancers. J Biol Chem. 2020;295(3):757-770.

41. Wang P, Wang Z, Liu J. Role of HDACs in normal and malignant hematopoiesis. Mol Cancer. 2020;19(1):5.

42. Thambyrajah R, Fadlullah MZH, Proffitt M, et al. HDAC1 and HDAC2 Modulate TGF-β Signaling during Endothelial-to-Hematopoietic Transition. Stem Cell Reports. 2018;10(4):1369-1383.

43. Ye M, Zhang H, Amabile G, et al. C/EBPa controls acquisition and maintenance of adult

haematopoietic stem cell quiescence. Nat Cell Biol. 2013;15(4):385-394.

44. Avellino R, Delwel R. Expression and regulation of C/EBPα in normal myelopoiesis and in malignant transformation. Blood. 2017;129(15):2083-2091.

45. Bedi R, Du J, Sharma AK, Gomes I, Ackerman SJ. Human C/EBP-epsilon activator and repressor isoforms differentially reprogram myeloid lineage commitment and differentiation. Blood. 2009;113(2):317-327.

46. Shyamsunder P, Shanmugasundaram M, Mayakonda A, et al. Identification of a novel enhancer of CEBPE essential for granulocytic differentiation. Blood. 2019;133(23):2507-2517.

47. Broughton SE, Dhagat U, Hercus TR, et al. The GM-CSF/IL-3/IL-5 cytokine receptor family: from ligand recognition to initiation of signaling. Immunol Rev. 2012;250(1):277-302.

48. Regan-Komito D, Swann JW, Demetriou P, et al. GM-CSF drives dysregulated hematopoietic stem cell activity and pathogenic extramedullary myelopoiesis in experimental spondyloarthritis. Nat Commun. 2020;11(1):155.

49. Naik SH, Perié L, Swart E, et al. Diverse and heritable lineage imprinting of early haematopoietic progenitors. Nature. 2013;496(7444):229-232.

50. Lin DS, Kan A, Gao J, Crampin EJ, Hodgkin PD, Naik SH. DiSNE Movie Visualization and Assessment of Clonal Kinetics Reveal Multiple Trajectories of Dendritic Cell Development. Cell Rep. 2018;22(10):2557-2566.

51. Feng J, Pucella JN, Jang G, et al. Clonal lineage tracing reveals shared origin of conventional and plasmacytoid dendritic cells. Immunity. 2022;55(3):405-422.e11.

52. Welner RS, Bararia D, Amabile G, et al. C/EBPα is required for development of dendritic cell progenitors. Blood. 2013;121(20):4073-4081.

53. Laiosa CV, Stadtfeld M, Graf T. Determinants of lymphoid-myeloid lineage diversification. Annu Rev Immunol. 2006;24:705-738.

54. Pascall JC, Webb LMC, Eskelinen EL, Innocentin S, Attaf-Bouabdallah N, Butcher GW. GIMAP6 is required for T cell maintenance and efficient autophagy in mice. PLoS One. 2018;13(5):e0196504.

55. Chu Y, Chen Y, Li M, et al. Six1 regulates leukemia stem cell maintenance in acute myeloid leukemia. Cancer Sci. 2019;110(7):2200-2210.

56. Manesia JK, Maganti HB, Almoflehi S, et al. AA2P-mediated DNA demethylation synergizes with stem cell agonists to promote expansion of hematopoietic stem cells. Cell Rep Methods.

2023;3(12):100663.

57. Stanford SM, Bottini N. Targeting protein phosphatases in cancer immunotherapy and autoimmune disorders. Nat Rev Drug Discov. 2023;22(4):273-294.

58. Tan W, Sunahori K, Zhao J, et al. Association of PPP2CA polymorphisms with systemic lupus erythematosus susceptibility in multiple ethnic groups. Arthritis Rheum. 2011;63(9):2755-2763.

59. Brinkmann V, Billich A, Baumruker T, et al. Fingolimod (FTY720): discovery and development of an oral drug to treat multiple sclerosis. Nat Rev Drug Discov. 2010;9(11):883-897.

Figure Legends

Figure 1. *Ppp2ca* modulates hematopoietic lineage commitment. *Ppp2ca*$^{f/f}$ (WT) or *Ert2*^{cre}*Ppp2ca*$^{f/f}$ (KO) mice were treated with tamoxifen for 5 consecutive days, and the phenotype was analyzed on day 10 following last treatment. (A) The splenomegaly observed in *Ppp2ca*-deficient mice. (B) The number of splenocytes. (C) The proportion of splenic B cells, CD4$^+$ T cells and CD8$^+$ T cells. (D) The proportion of splenic granulocytes (Granu), monocytes (Mono) and macrophages (Macro). (E) The proportion of splenic pDC, cDC1 and cDC2. (F) The number of splenic B cells, CD4$^+$ T cells and CD8$^+$ T cells. (G) The number of splenic granulocytes, monocytes and macrophages. (H) The number of splenic pDC, cDC1 and cDC2. (I) The number of total BM cells. (J-L) The proportion of B cells (J), granulocytes (K) and monocytes (L) in the BM. (M-O) The number of B cells (M), granulocytes (N) and monocytes (O) in the BM. (P) The number of BM lineage negative (Lin$^-$) cells. (Q) The proportion of GMP, CMP and MEP in BM Lin$^-$ cells. (R) The proportion of CLP in BM Lin$^-$ cells. (S) The number of CLP. n=6-7. For B,I-P,R,S, *p* values were determined by a two-tailed unpaired *t* test. For C-H,Q, *p* values were determined by two-way ANOVA followed by Bonferroni post-hoc test. Data are presented as mean±SEM. (*p<0.05, **p<0.01, ***p<0.001, n.s., not significant).

Figure 2. *Ppp2ca* deficiency leads to dysregulated expression of genes involved in hematopoietic and metabolic pathways. LSK cells, isolated from the BM of tamoxifen pre-treated *Ppp2ca*$^{f/f}$ (WT) and *Ert2*^{cre}*Ppp2ca*$^{f/f}$ (KO) mice, were subjected to RNA-seq. (A) KEGG analysis of downregulated genes in *Ppp2ca* KO LSK. (B) A heatmap showing the changes in the expression of genes related to the hematopoietic lineage. (C) KEGG analysis of upregulated genes in *Ppp2ca* KO LSK. (D) Heatmap depicting the alterations in the expression levels of genes associated with energy metabolism. (E–G) GSEA analysis was performed to identify gene sets enriched in T cell differentiation, B cell differentiation and myeloid cell differentiation (E); glycolysis and oxidative phosphorylation pathways (F); and the MTORC1 signaling pathway, Myc target genes, and myeloid CEBPA network (G). n=3.

Figure 3. *Ppp2ca* deficiency leads to metabolic abnormalities. LSK cells were isolated from the BM of tamoxifen pre-treated *Ppp2ca*$^{f/f}$ (WT) and *Ert2*^{cre}*Ppp2ca*$^{f/f}$ (KO) mice, and then subjected to LC-MS/MS analysis. (A) Overview of metabolomics. Metabolites increased in *Ppp2ca*-deficient LSK cells are represented in purple color. Metabolic genes upregulated in *Ppp2ca*-deficient LSK cells are indicated in red color. Decreased metabolites and metabolic genes are shown in dark blue. (B) Heatmap depicting the alteration in the levels of metabolites. n=3. (C) Analysis of extracellular acidification rate (ECAR) and glycolytic capacity of LSK cells. n=6. (D) The levels of lactate in LSK cells. n=3. (E) The ratios of NAD^+ to NADH. n=3. (F) The levels of total ROS (tROS), cytosolic ROS (cytoROS) and mitochondrial ROS (mitoROS) in LSK cells. n=4-8. Data are representative of three independent experiments. *p* values were determined by a two-tailed unpaired *t* test. Data are presented as mean±SEM. (*p<0.05, **p<0.01, ***p<0.001).

Figure 4. *Ppp2ca* keeps the transcription of glycolytic genes in check. LSK cells were isolated from the BM of WT mice, and subjected to CUT&Tag analysis. (A) Enriched metabolic pathways of genes associated with the binding loci of PPP2CA. (B) The genomic browser track presenting the PPP2CA signal at the loci of representative target genes. The blue rectangles indicate the peak regions of PPP2CA occupancy on the promoters of target genes. Repeated experiments are presented. rep, repeat. (C) LSK cells isolated from the BM of tamoxifen pre-treated *Ppp2ca*$^{f/f}$ (WT) and *Ert2*^{cre}*Ppp2ca*$^{f/f}$ (KO) mice were subjected to CHIP-qPCR analysis. The occupancy of $pSer^5$ at the promoter of target genes is shown. $pSer^5$, a well-recognized marker of transcription initiation. n=3. *p* values were determined by a two-tailed unpaired *t* test. Data are presented as mean±SEM. (**p<0.01, ***p<0.001, n.s., not significant).

Figure 5. Haploid deletion of *Ldha* gene alleviates the abnormal hematopoiesis in *Ppp2ca*-deficient mice. (A) The levels of L-lactate in the Lin^- cells of BM. *p* values were determined by one-way ANOVA followed by Tukey's honestly significant difference (HSD) post-hoc test. Data are presented as mean±SEM. n=5-9. (***p<0.001, n.s., not significant). (B) The proportion of B cells, pDCs, granulocytes (Granu) and monocytes (Mono) in the BM. (C) The proportion of B cells, T cells, granulocytes, monocytes, macrophages (Macro), cDC1, cDC2 and pDC in the spleen. (D) The proportion of CLP, CMP, GMP and MEP in the BM. n=5-9. *p* values were

determined by two-way ANOVA followed by Bonferroni post-hoc test. Data are presented as mean±SEM. (*p<0.05, **p<0.01, ***p<0.001, n.s., not significant).

Figure 6. Increased lactylation of HDAC1 and HDAC2 upon deletion of *Ppp2ca*. (A) LSK cells were prepared from the BM of tamoxifen pre-treated *Ppp2ca*$^{f/f}$ (WT) and *Ert2*^{cre}*Ppp2ca*$^{f/f}$ (KO) mice. Statistical analysis of lactylated sites and proteins. (B) Heatmap depicting the increased lactylation levels of proteins involved in hematopoiesis. n=3. (C) Mass spectrometry analysis of the lactylated HDAC peptides (HDAC1K412la and HDAC2K451la). 'b' refers to the amino-terminal parts of the peptide and 'y' refers to the carboxy-terminal parts of the peptide. Data represent three independent experiments. (D) The conservation of lactylated sites in HDAC1 and HDAC2. (E) Lin$^-$ cells isolated from the BM of tamoxifen treated *Ppp2ca*$^{f/f}$ (*P*$^{f/f}$) *and Ert2*^{cre}*Ppp2ca*$^{f/f}$ (*E*^{cre}*P*$^{f/f}$) mice were incubated with or without oxamate (Oxa). Subsequently, intracellular HDAC1 and HDAC2 were respectively immunoprecipitated (IP) with anti-HDAC1 and anti-HDAC2 antibodies, followed by detection of lactylation using anti-lactyllysine antibody (anti-Kla). (F) Immunoblot analysis assessing the pan-lysine acetylation (anti-Kac) levels in LSK. Coomassie blue staining (CB) indicates equal loading of protein. (G) Analysis of the site specific lactylation of HDAC1 and HDAC2. Cell lysates from Lin$^-$ cells with HDAC1-Flag or HDAC2-Flag overexpressing were subjected to immunoprecipitation using an anti-Flag antibody (anti-Flag), followed by detection of lactylation with an anti-lactyllysine antibody (anti-Kla). The relative ratios of lactyl-HDAC to total-HDAC and total-HDAC to β-ACTIN are shown. The experiments were repeated for three times. *p* values were determined by a two-tailed unpaired *t* test. Data are presented as mean±SEM. (*p<0.05, n.s., not significant).

Figure 7. Enhanced lactylation of HDACs contributes to the excessive expression of myeloid determining genes following *Ppp2ca* deletion. (A, C) Lin$^-$ cells were transfected with the lentiviral constructs encoding HDAC1-K412-Flag (K412), HDAC1-R412-Flag (R412), HDAC2-K451-Flag (K451) or HDAC2-R451-Flag (R451). (A) Overexpressed HDACs were immunoprecipitated with anti-Flag antibody. The deacetylase activity of HDAC1 and HDAC2 was detected. n=3. *p* values were determined by one-way ANOVA followed by Tukey's post-hoc test. Data are presented as mean±SEM. (n.s., not significant). (B) Schematic diagram of the structural domains of HDAC1 and

HDAC2. (C) The impact of site-specific HDAC lactylation on the assembly of SIN3A/HDAC complex. Overexpressed HDAC proteins were immunoprecipitated (IP) with anti-Flag antibody, and associated proteins were detected by immunoblotting. Data are representative of three independent experiments. (D) LSK cells isolated from the BM of tamoxifen pre-treated *Ppp2ca*$^{f/f}$ (WT) and *Ert2*^{cre}*Ppp2ca*$^{f/f}$ (KO) mice were subjected to CHIP-qPCR analysis. The relative enrichment of H3K27ac at the promoter of target genes is shown. n=6. *p* values were determined by a two-tailed unpaired *t* test. Data are presented as mean±SEM. (***p<0.001, ****p<0.0001. n.s., not significant). (E) LSK cells were prepared from the BM of tamoxifen treated *Ppp2ca*$^{f/f}$ (*P*$^{f/f}$) *and Ert2*^{cre}*Ppp2ca*$^{f/f}$ (*E*^{cre}*P*$^{f/f}$) mice, and then incubated with oxamate (Oxa). The acetylation level of histone H3 at lysine 27 (H3K27ac) was assessed by immunoblotting. β-ACTIN was used as the internal loading control. Data are representative of three independent experiments. *p* values were determined by one-way ANOVA followed by Tukey's post-hoc test. Data are presented as mean±SEM. (*p<0.05, ***p<0.001, n.s., not significant). (F) Immunoblot analysis of the LDHA and H3K27ac levels in the BM LSK cells from *Ppp2ca*$^{f/f}$, *Ert2*^{cre}*Ppp2ca*$^{f/f}$, *Ppp2ca*$^{f/f}$*Ldha*$^{f/+}$ and *Ert2*^{cre}*Ppp2ca*$^{f/f}$*Ldha*$^{f/+}$ mice.

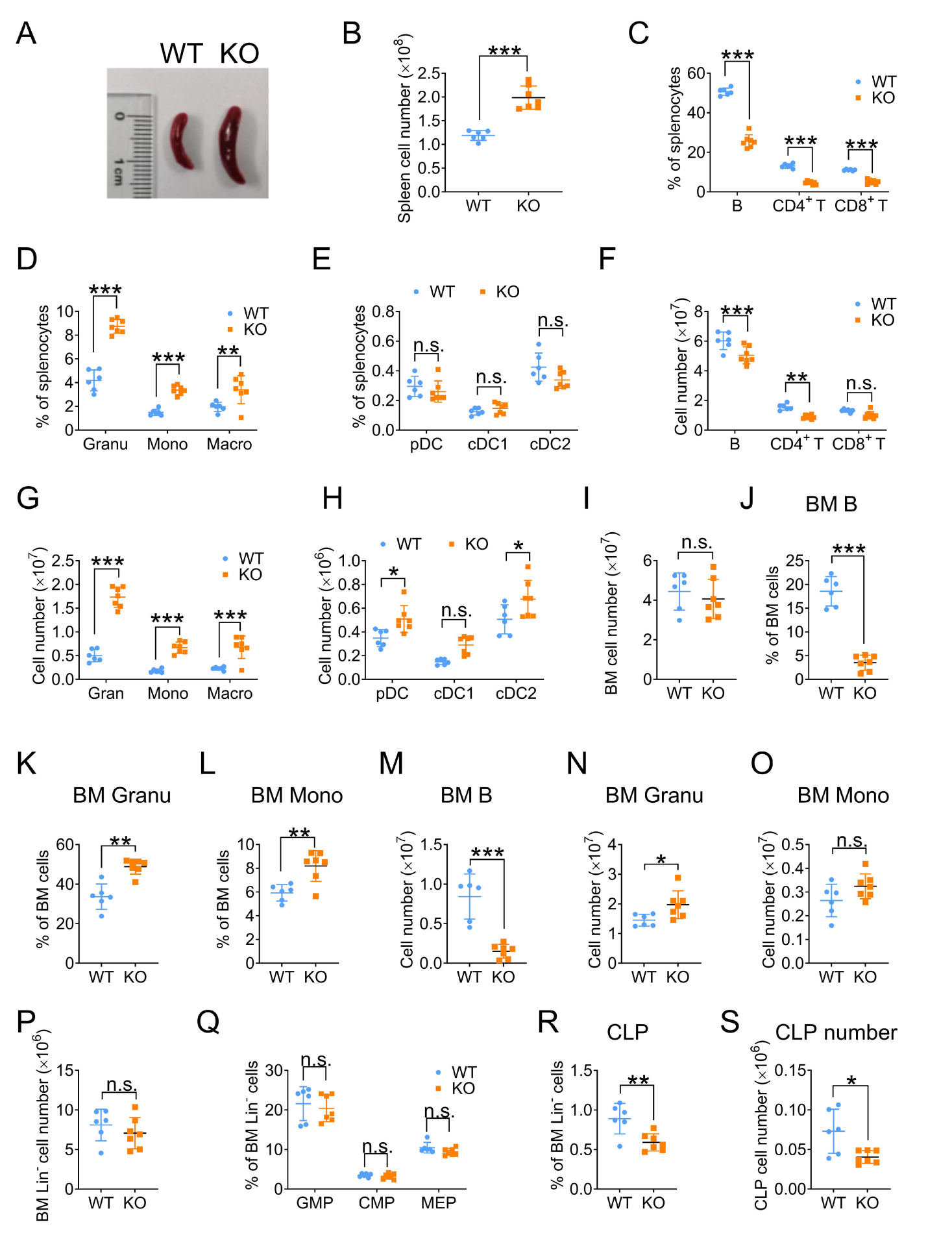
A
WT KO
B
Spleen cell number (×10^8)
***
WT KO
C
% of splenocytes
***
***
***
WT
KO
B
CD4+ T
CD8+ T
D
% of splenocytes
***
***
**
WT
KO
Granu
Mono
Macro
E
% of splenocytes
WT
KO
n.s.
n.s.
n.s.
pDC
cDC1
cDC2
F
Cell number (×10^7)
***
**
n.s.
WT
KO
B
CD4+ T
CD8+ T
G
Cell number (×10^7)
***
***
***
WT
KO
Gran
Mono
Macro
H
Cell number (×10^6)
WT
KO
*
n.s.
*
pDC
cDC1
cDC2
I
BM cell number (×10^7)
n.s.
WT KO
J
BM B
% of BM cells
***
WT KO
K
BM Granu
% of BM cells
**
WT KO
L
BM Mono
% of BM cells
**
WT KO
M
BM B
Cell number (×10^7)
***
WT KO
N
BM Granu
Cell number (×10^7)
*
WT KO
O
BM Mono
Cell number (×10^7)
n.s.
WT KO
P
BM Lin- cell number (×10^6)
n.s.
WT KO
Q
% of BM Lin- cells
n.s.
n.s.
n.s.
WT
KO
GMP
CMP
MEP
R
CLP
% of BM Lin- cells
**
WT KO
S
CLP number
CLP cell number (×10^6)
*
WT KO

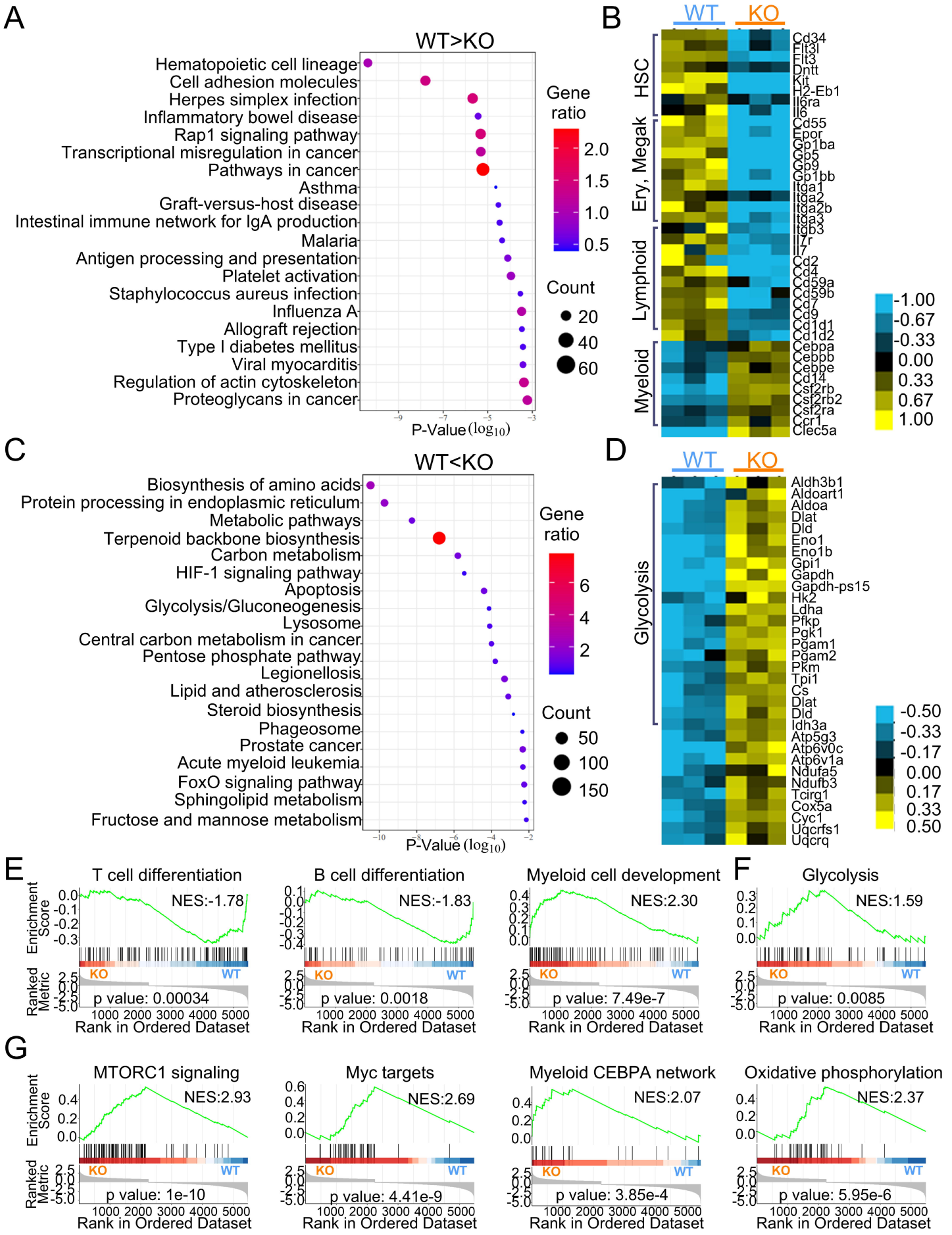
A
WT>KO
Hematopoietic cell lineage
Cell adhesion molecules
Herpes simplex infection
Inflammatory bowel disease
Rap1 signaling pathway
Transcriptional misregulation in cancer
Pathways in cancer
Asthma
Graft-versus-host disease
Intestinal immune network for IgA production
Malaria
Antigen processing and presentation
Platelet activation
Staphylococcus aureus infection
Influenza A
Allograft rejection
Type I diabetes mellitus
Viral myocarditis
Regulation of actin cytoskeleton
Proteoglycans in cancer
P-Value (log10)
Gene ratio
Count
B
WT
KO
HSC
Ery, Megak
Lymphoid
Myeloid
Cd34
Flt3l
Flt3
Dntt
Kit
H2-Eb1
Il6ra
Il6
Cd55
Epor
Gp1ba
Gb5
Gp9
Gp1bb
Itga1
Itga2
Itga2b
Itga3
Itgb3
Il7r
Il7
Cd2
Cd4
Cd59a
Cd59b
Cd7
Cd9
Cd1d1
Cd1d2
Cebpa
Cebpb
Cebpe
Cd14
Csf2rb
Csf2rb2
Csf2ra
Ccr1
Clec5a
C
WT<KO
Biosynthesis of amino acids
Protein processing in endoplasmic reticulum
Metabolic pathways
Terpenoid backbone biosynthesis
Carbon metabolism
HIF-1 signaling pathway
Apoptosis
Glycolysis/Gluconeogenesis
Lysosome
Central carbon metabolism in cancer
Pentose phosphate pathway
Legionellosis
Lipid and atherosclerosis
Steroid biosynthesis
Phageosome
Prostate cancer
Acute myeloid leukemia
FoxO signaling pathway
Sphingolipid metabolism
Fructose and mannose metabolism
P-Value (log10)
Gene ratio
Count
D
WT
KO
Glycolysis
Aldh3b1
Aldoart1
Aldoa
Dlat
Dld
Eno1
Eno1b
Gpi1
Gapdh
Gapdh-ps15
Hk2
Ldha
Pfkp
Pgk1
Pgam1
Pgam2
Pkm
Tpi1
Cs
Dlat
Dld
Idh3a
Atp5g3
Atp6v0c
Atp6v1a
Ndufa5
Ndufb3
Tcirg1
Cox5a
Cyc1
Uqcrfs1
Uqcrq
E
T cell differentiation
NES:-1.78
p value: 0.00034
B cell differentiation
NES:-1.83
p value: 0.0018
Myeloid cell development
NES:2.30
p value: 7.49e-7
F
Glycolysis
NES:1.59
p value: 0.0085
Enrichment Score
Ranked Metric
KO
WT
Rank in Ordered Dataset
G
MTORC1 signaling
NES:2.93
p value: 1e-10
Myc targets
NES:2.69
p value: 4.41e-9
Myeloid CEBPA network
NES:2.07
p value: 3.85e-4
Oxidative phosphorylation
NES:2.37
p value: 5.95e-6

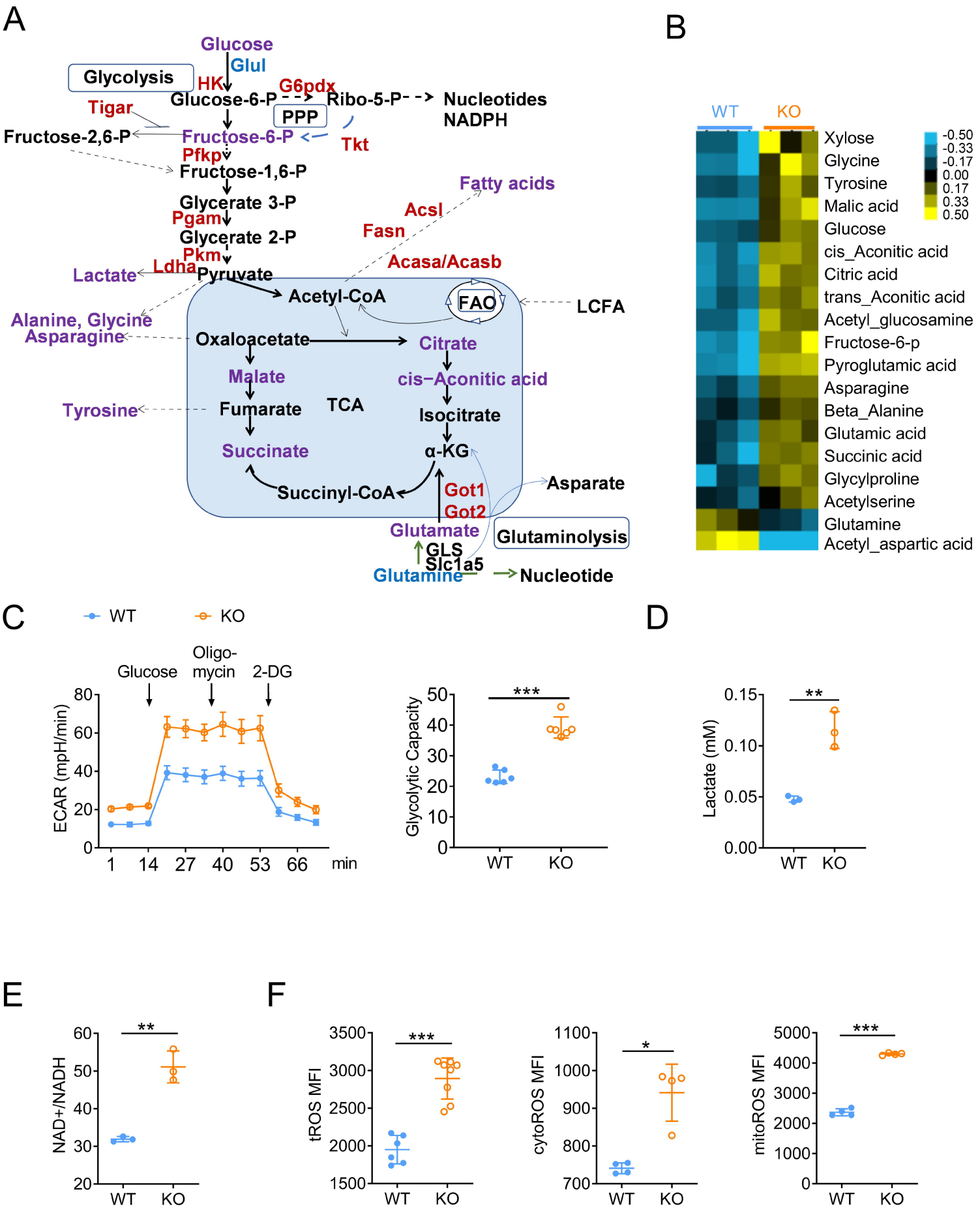
A
Glucose
Glul
Glycolysis
HK
G6pdx
Glucose-6-P
Ribo-5-P
Nucleotides
NADPH
PPP
Tigar
Fructose-2,6-P
Fructose-6-P
Tkt
Pfkp
Fructose-1,6-P
Fatty acids
Acsl
Fasn
Glycerate 3-P
Pgam
Glycerate 2-P
Pkm
Ldha
Lactate
Pyruvate
Acasa/Acasb
Acetyl-CoA
FAO
LCFA
Alanine, Glycine
Asparagine
Oxaloacetate
Citrate
Malate
cis−Aconitic acid
Tyrosine
Fumarate
TCA
Isocitrate
Succinate
α-KG
Succinyl-CoA
Got1
Got2
Asparate
Glutamate
Glutaminolysis
GLS
Slc1a5
Glutamine
Nucleotide
B
WT
KO
Xylose
Glycine
Tyrosine
Malic acid
Glucose
cis_Aconitic acid
Citric acid
trans_Aconitic acid
Acetyl_glucosamine
Fructose-6-p
Pyroglutamic acid
Asparagine
Beta_Alanine
Glutamic acid
Succinic acid
Glycylproline
Acetylserine
Glutamine
Acetyl_aspartic acid
-0.50
-0.33
-0.17
0.00
0.17
0.33
0.50
C
WT
KO
Glucose
Oligo-mycin
2-DG
ECAR (mpH/min)
min
Glycolytic Capacity
***
D
Lactate (mM)
**
E
NAD+/NADH
**
F
tROS MFI
***
cytoROS MFI
*
mitoROS MFI
***

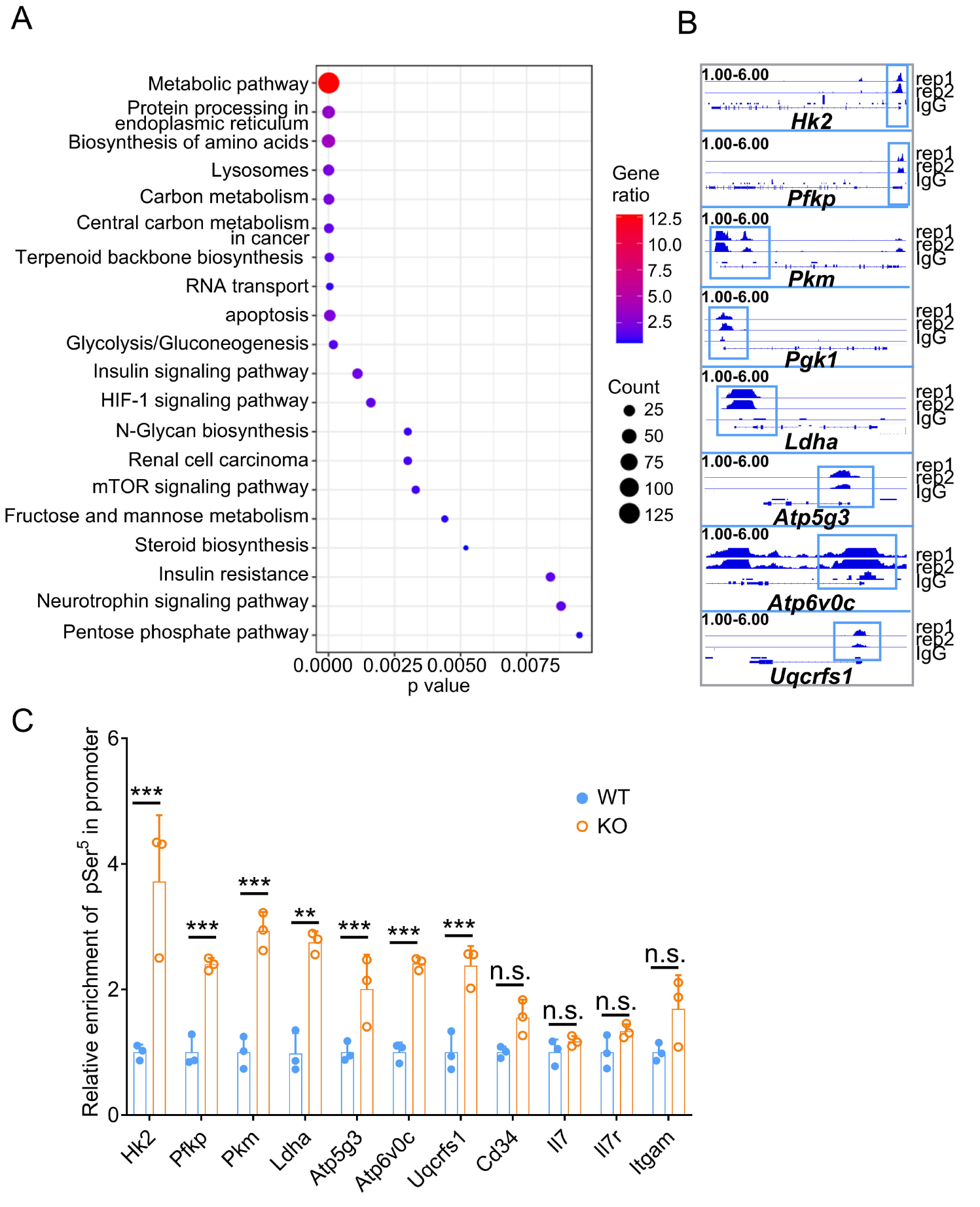
A
Metabolic pathway
Protein processing in endoplasmic reticulum
Biosynthesis of amino acids
Lysosomes
Carbon metabolism
Central carbon metabolism in cancer
Terpenoid backbone biosynthesis
RNA transport
apoptosis
Glycolysis/Gluconeogenesis
Insulin signaling pathway
HIF-1 signaling pathway
N-Glycan biosynthesis
Renal cell carcinoma
mTOR signaling pathway
Fructose and mannose metabolism
Steroid biosynthesis
Insulin resistance
Neurotrophin signaling pathway
Pentose phosphate pathway
0.0000 0.0025 0.0050 0.0075
p value
Gene ratio
12.5
10.0
7.5
5.0
2.5
Count
25
50
75
100
125
B
1.00-6.00
rep1
rep2
IgG
Hk2
Pfkp
Pkm
Pgk1
Ldha
Atp5g3
Atp6v0c
Uqcrfs1
C
Relative enrichment of pSer5 in promoter
0
2
4
6
WT
KO
***
***
***
**
***
***
***
n.s.
n.s.
n.s.
n.s.
Hk2
Pfkp
Pkm
Ldha
Atp5g3
Atp6v0c
Uqcrfs1
Cd34
Il7
Il7r
Itgam

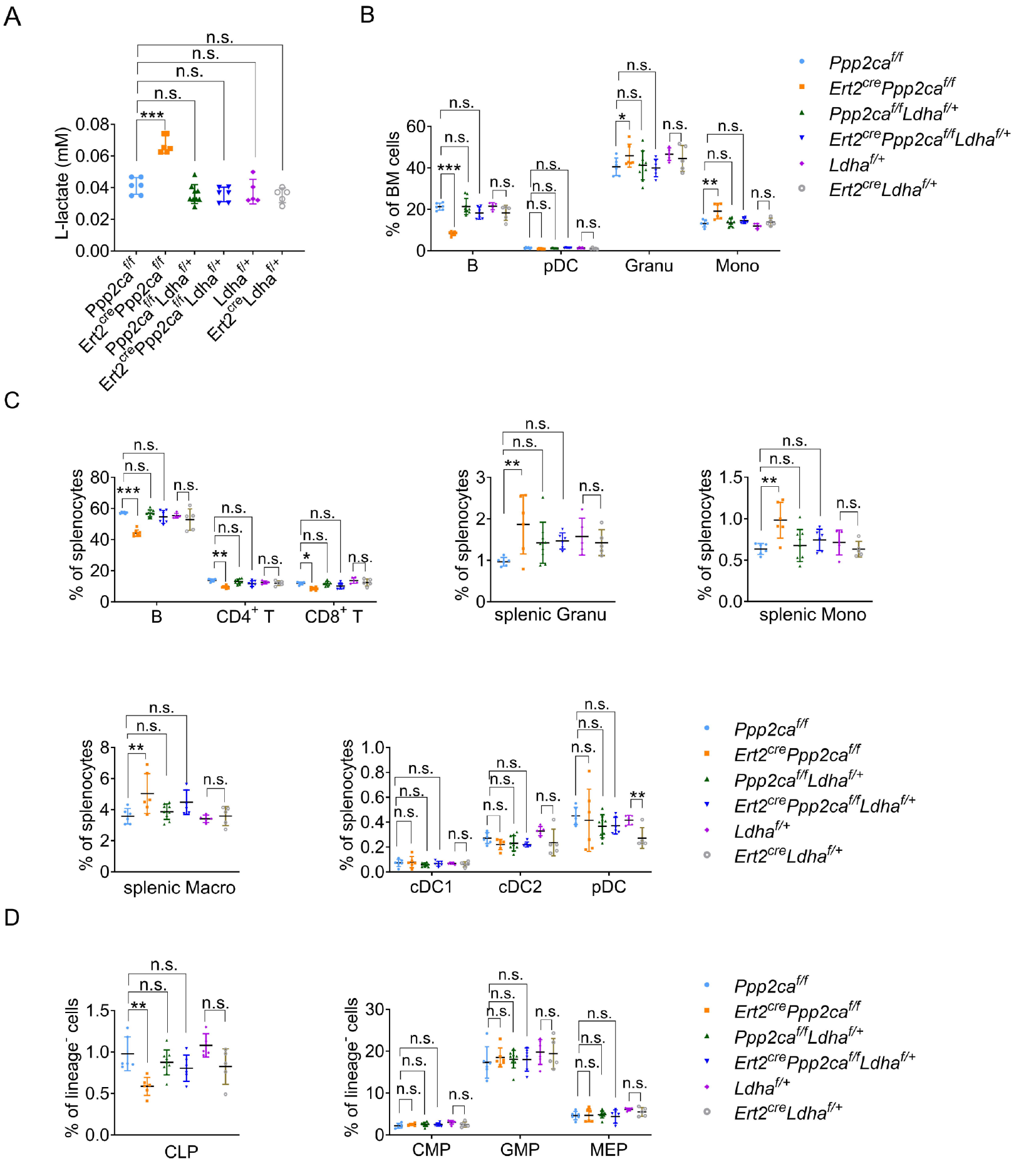
A
B
C
D
L-lactate (mM)
% of BM cells
% of splenocytes
% of lineage⁻ cells
B
pDC
Granu
Mono
CD4+ T
CD8+ T
splenic Granu
splenic Mono
splenic Macro
cDC1
cDC2
pDC
CLP
CMP
GMP
MEP
n.s.
Ppp2ca f/f
Ert2cre Ppp2ca f/f
Ppp2ca f/f Ldha f/+
Ert2cre Ppp2ca f/f Ldha f/+
Ldha f/+
Ert2cre Ldha f/+

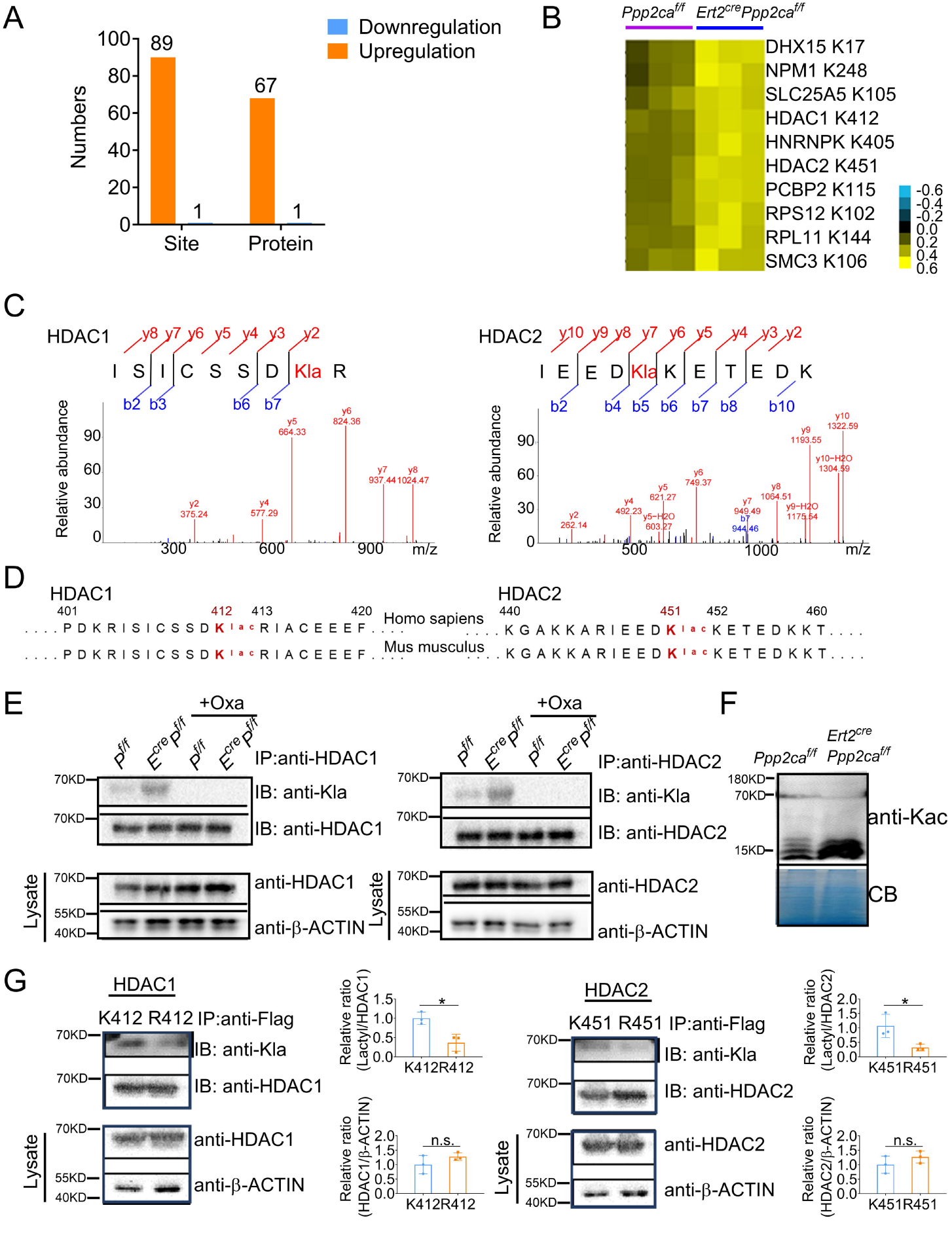
A
Downregulation
Upregulation
Numbers
100
80
60
40
20
0
89
1
67
1
Site
Protein
B
Ppp2ca f/f
Ert2cre Ppp2ca f/f
DHX15 K17
NPM1 K248
SLC25A5 K105
HDAC1 K412
HNRNPK K405
HDAC2 K451
PCBP2 K115
RPS12 K102
RPL11 K144
SMC3 K106
-0.6
-0.4
-0.2
0.0
0.2
0.4
0.6
C
HDAC1
I S I C S S D Kla R
b2 b3 b6 b7
y8 y7 y6 y5 y4 y3 y2
Relative abundance
m/z
HDAC2
I E E D Kla K E T E D K
b2 b4 b5 b6 b7 b8 b10
y10 y9 y8 y7 y6 y5 y4 y3 y2
D
HDAC1
HDAC2
Homo sapiens
Mus musculus
E
+Oxa
P f/f
E cre P f/f
IP:anti-HDAC1
IB: anti-Kla
IB: anti-HDAC1
IP:anti-HDAC2
IB: anti-HDAC2
Lysate
anti-HDAC1
anti-HDAC2
anti-β-ACTIN
70KD
55KD
40KD
F
Ppp2ca f/f
Ert2cre Ppp2ca f/f
180KD
70KD
15KD
anti-Kac
CB
G
HDAC1
K412 R412 IP:anti-Flag
IB: anti-Kla
IB: anti-HDAC1
anti-HDAC1
anti-β-ACTIN
Relative ratio (Lacyl/HDAC1)
K412R412
Relative ratio (HDAC1/β-ACTIN)
HDAC2
K451 R451 IP:anti-Flag
IB: anti-HDAC2
anti-HDAC2
Relative ratio (Lacyl/HDAC2)
K451R451
Relative ratio (HDAC2/β-ACTIN)
n.s.

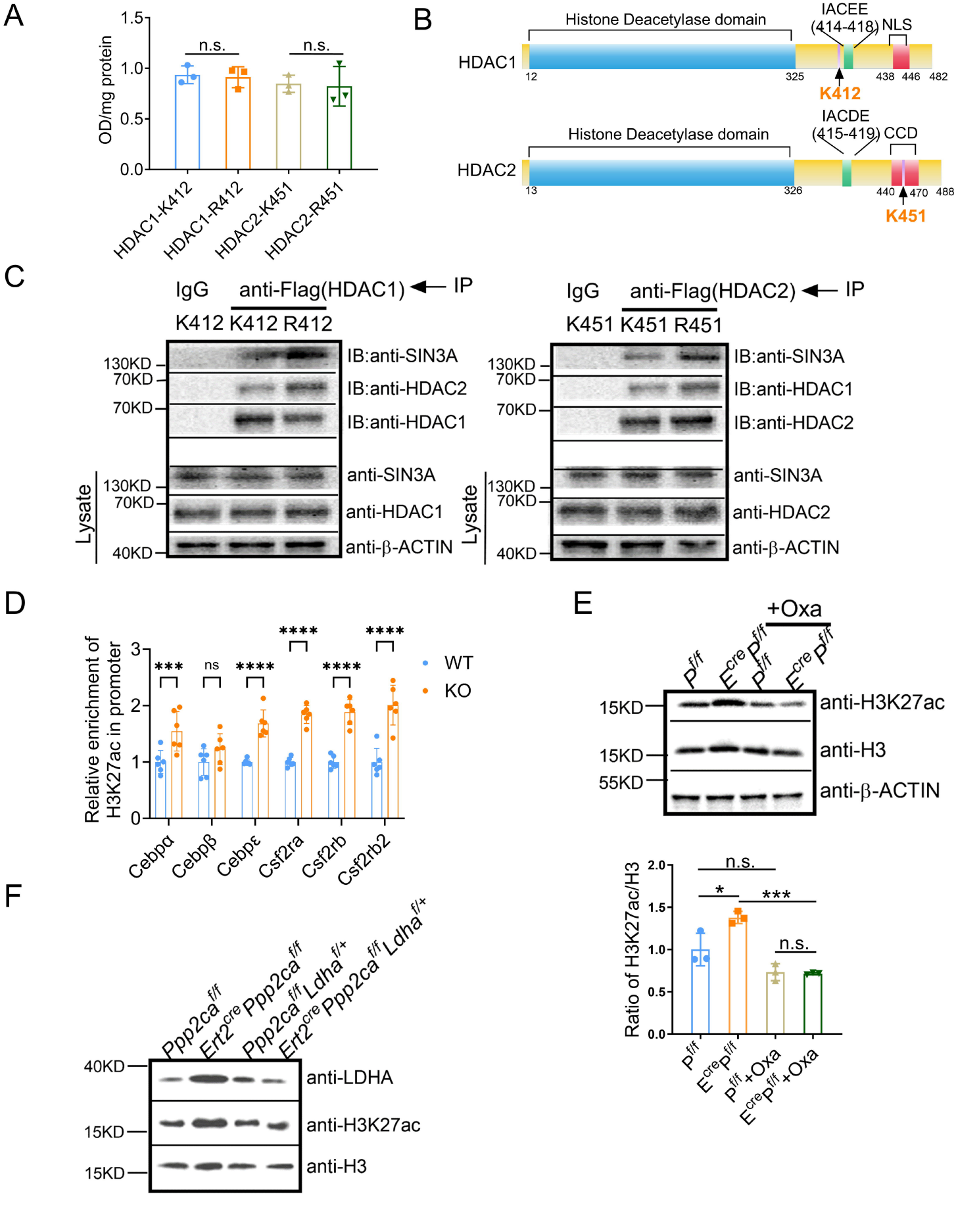
A
OD/mg protein
1.5
1.0
0.5
0.0
n.s.
n.s.
HDAC1-K412
HDAC1-R412
HDAC2-K451
HDAC2-R451
B
Histone Deacetylase domain
IACEE
(414-418)
NLS
HDAC1
12
325
438
446
482
K412
Histone Deacetylase domain
IACDE
(415-419)
CCD
HDAC2
13
326
440
470
488
K451
C
IgG
anti-Flag(HDAC1)
IP
K412 K412 R412
130KD
70KD
70KD
IB:anti-SIN3A
IB:anti-HDAC2
IB:anti-HDAC1
Lysate
130KD
70KD
anti-SIN3A
anti-HDAC1
40KD
anti-β-ACTIN
IgG
anti-Flag(HDAC2)
IP
K451 K451 R451
130KD
70KD
70KD
IB:anti-SIN3A
IB:anti-HDAC1
IB:anti-HDAC2
Lysate
130KD
70KD
anti-SIN3A
anti-HDAC2
40KD
anti-β-ACTIN
D
Relative enrichment of H3K27ac in promoter
3
2
1
0
***
ns
****
****
****
****
WT
KO
Cebpα
Cebpβ
Cebpε
Csf2ra
Csf2rb
Csf2rb2
E
+Oxa
P f/f
E cre P f/f
P f/f
E cre P f/f
15KD
anti-H3K27ac
15KD
anti-H3
55KD
anti-β-ACTIN
Ratio of H3K27ac/H3
2.0
1.5
1.0
0.5
0.0
n.s.
*
***
n.s.
P f/f
E cre P f/f
P f/f +Oxa
E cre P f/f +Oxa
F
Ppp2ca f/f
Ert2 cre Ppp2ca f/f
Ppp2ca f/f Ldha f/+
Ert2 cre Ppp2ca f/f Ldha f/+
40KD
anti-LDHA
15KD
anti-H3K27ac
15KD
anti-H3

Supplementary Methods

Cell preparation and flow cytometry analysis

Single cells from murine spleen and BM were prepared as previously described. Briefly, splenocytes were enzymatically digested with 1 mg/mL collagenase IV (C5138, Sigma-Aldrich) and 10 μg/mL DNase I (10104159001, Roche) at 37°C for 30 min. Red blood cells were then lysed using red cell lysis buffer (00-4333-57, ThermoFisher Scientific). Single-cell suspensions were prepared by passing through a 70-μm cell strainer. To block non-specific binding, cells were incubated with anti-mouse CD16/32 antibody (101302, BioLegend, 1:200) at 4°C for 15 min. Cells were subsequently stained with fluorochrome-conjugated antibodies (1:200) for 30 min at 4°C in the dark, followed by washing with PBS. For live-cell discrimination, cells were stained with BD Horizon™ Fixable Viability Stain 575V (565694, BD Biosciences, 1:1000) at room temperature for 10 min. After washing with staining buffer (420210, BioLegend), cells were analyzed using a BD LSRFortessa flow cytometer, and data were processed with FlowJo v10 software. A detailed list of antibodies used in this study is provided in Supplementary Table 1.

Lin^- cells were obtained by depleting lineage cells using a combination of rat-anti-mouse antibody cocktails (CD2, CD3, CD8, CD11b, Gr-1, Ter-119, CD19, B220) and anti-rat secondary antibody conjugated with magnetic beads (Biomag).

ROS analysis via flow cytometry

Total ROS levels in BM LSK cells were detected using CellROX™ Green Reagent (C10492, ThermoFisher Scientific). Cytosolic and mitochondrial ROS was detected with DCFH-DA (cytosolic ROS-preferential probe, Catalog No.: C6827, ThermoFisher Scientific) and MitoSOX™ Red Reagent (mitochondrial ROS-specific probe, Catalog No.: M36008, ThermoFisher Scientific), respectively. Isolated BM LSK cells (2×10^5) were resuspended in 200 μL serum-free RPMI 1640 medium and incubated with 500 nM CellROX™ Green Reagent, 500 nM MitoSOX™ Red Reagent or 1 μM DCFH-DA at 37°C for 30 min in the dark. After two washes with PBS, cells were immediately analyzed by flow cytometry (BD LSRFortessa). The mean fluorescence intensity (MFI) of CellROX™ Green, MitoSOX™ Red and DCFH-DA was recorded to quantify total, mitochondrial, and cytosolic ROS levels, respectively.

Measurement of NAD+/NADH ratio

The NAD+/NADH ratio in BM LSK cells was determined using the NAD+/NADH Assay Kit (ab176723, Abcam) following the manufacturer's instructions. Briefly, 1×10^6 BM LSK cells were collected and lysed in 25 μL of the provided lysis buffer for 10 min. After centrifugation at 400 × g for 5 min, the supernatant was transferred to a 96-well plate. For each sample well, 25 μL of NAD or NADH extraction solution was added, followed by 75 μL of reaction mixture. The plate was incubated at 37°C for 1 h, and absorbance was measured at a wavelength of 576 ± 5 nm using a colorimetric microplate reader. The NAD+/NADH ratio was calculated based on the

standard curve generated with the provided standard solutions. All experiments were performed in triplicate.

Cell culture and transfection

LSK or Lin^- cells were cultured in Roswell Park Memorial Institute (RPMI) 1640 (Gibco) containing L-glutamine, supplemented with 10% Fetal Bovine Serum (FBS, Gibco), 1% Penicillin-Streptomycin (Gibco) and 0.1% 2-Mercaptoethanol (Gibco). Lin^- cells were treated with or without 10mM sodium oxamate (Selleck). 293FT cell line was cultured in Dulbecco's Modified Eagle Medium (DMEM, Gibco) containing L-glutamine supplemented with 10% FBS (Gibco) and 1% Penicillin-Streptomycin (Gibco).

For lentiviral transfection, mouse Lin^- cells were pre-stimulated with 100ng/mL SCF, 100ng/mL Flt3L and 100ng/mL TPO for 24 hours. Then, cells were subjected to centrifugal transfection at 37℃, 1000g for 1 hour. After that, cells were washed and prepared for subsequent studies.

Plasmid construction

The coding regions of murine HDAC1 (NM_008228) and HDAC2 (NM_008229) were synthesized and cloned into the multiple cloning sites of the EF1α-MCS-Flag-PGK-EGFP lentiviral plasmid (Tsingke Biotech, China). The mutant forms of HDAC1 and HDAC2 were constructed by using the KOD -Plus-

Mutagenesis Kit (TOYOBO, Japan).

RNA sequencing

Total RNA was extracted by Trizol reagent (Invitrogen). RNA libraries were prepared using the VAHTS mRNA-seq v2 Library Prep Kit for Illumina® (Vazyme, Nanjing, China) and sequenced on the Novaseq 6000 system (Illumina, San Diego, CA, USA). Genes with *p* value less than 0.05, as determined by DESeq2 analysis, and log2 fold change greater than 0.5 were selected for further analysis. Kyoto Encyclopedia of Genes and Genomes (KEGG), Gene Ontology (GO) and Gene Set Enrichment Analysis (GSEA) were used to determine the enriched pathway of selected genes.

Immunoblots and co-immunoprecipitation

3×10^6 primary cells were lysed using RIPA protein exaction buffer (Thermo Fisher Scientific). Subsequently, the cell lysates (10μg/lane) were separated by 10% SDS-PAGE and transferred onto an Immobilon-P polyvinylidene difluoride membrane (Millipore, Billerica, MA). Then, the membrane was blocked with SuperBlock TBS blocking buffer (Thermo Fisher Scientific) and incubated with indicated antibodies listed in the Supplementary Table 1. Gels analysis was performed using Image J software.

Lysates were prepared from 1×10^7 cells transfected with HDAC1-Flag or HDAC2-Flag, followed by immunoprecipitation of HDAC protein using an anti-Flag

antibody (Cell Signaling Technology) and the Pierce™Classic Magnetic IP/Co-IP Kit (Thermo Fisher Scientific). The precipitated protein was detected by immunoblotting.

CUT&Tag and CUT&RUN

A total of 1×10^5 LSK cells were prepared by using the Hyperactive Universal CUT&Tag Assay Kit for Illumina (Vazyme, China) according to the protocol. The trimmomatic software was employed to remove adapters and low quality reads[24]. Before read mapping, clean reads were obtained from the raw reads by removing the adaptor sequences. The clean reads were then aligned to the GRCm38/mm10 genome sequences using the bwa program. The bam files were subjected to macs2 software for peak calling with cut off q value < 0.05. Reads distributions across peaks or genes were analyzed with the deeptools. The HOMER's findMotifsGenome.pl tool was used for motif analysis and peaks were annotated by ChIPseeker. For CUT&RUN, LSK cells were subjected to the Hyperactive pG-MNase CUT&RUN Assay Kit for Illumina (Vazyme, China). H3K27ac occupied sites with more than 1 fold change and *p* values less than 0.05 were selected for further analysis.

Metabolomics study

The metabolites in LSK cells were detected using the Q300 Kit provided by Metabo-Profile (Shanghai, China). Cell samples previously stored at −80℃ were subjected to a quantitative UPLC-MS/MS platform (ACQUITY UPLC-Xevo TQ-S, Waters Corp., MA, USA). The raw data files generated by UPLC-MS/MS were

processed using the TMBQ software (v1.0, Metabo-Profile, Shanghai, China) to perform peak integration, calibration, and quantitation for each metabolite. The XploreMET platform (version 4.0; Metabo-Profile, Shanghai, China) was used for statistical analysis, including principal component analysis (PCA), orthogonal partial least squares discriminant analysis (OPLS-DA), univariate analysis and pathway analysis.

Lactylation modified proteomics

The sample was grinded into cell powder with liquid nitrogen and lysed, followed by sonication for three minutes on ice using a high intensity ultrasonic processor (Scientz). Then, the supernatant was collected and protein was precipitated with the final concentration of 20% (m/v) TCA. The protein digestion was conducted overnight with the addition of trypsin at a trypsin-to-protein mass ratio of 1:50, followed by the peptides collection using Strata X SPE column. To enrich modified peptides, tryptic peptides dissolved in NETN buffer (100 mM NaCl, 1 mM EDTA, 50 mM Tris-HCl, 0.5% NP-40, pH 8.0) were incubated overnight at 4℃ with pre-washed agarose beads conjugated with anti-L-lactyllysine antibody (PTM Bio, PTM-1404). The bound peptides were eluted from the beads with 0.1% trifluoroacetic acid. For LC-MS/MS analysis, the obtained peptides were desalted with C18 ZipTips (Millipore) and dissolved in solvent A before being directly loaded onto a home-made reversed-phase analytical column (25-cm length, 100 μm i.d.). The mobile phase consisted of solvent A (0.1% formic acid, 2% acetonitrile/in water) and solvent B

(0.1% formic acid in acetonitrile). Peptides were separated with following gradient: 0-40 min, 6%-24% B; 40-52 min, 24%-35% B; 52-56 min, 35%-80% B; 56-60 min, 80% B, and all at a constant flow rate of 450nl/min on a NanoElute UHPLC system (Bruker Daltonics). Finally, peptides were subjected to capillary source followed by the timsTOF Pro mass spectrometry.

The MS/MS data were processed using the Maxquant search engine (v.1.6.15.0). Tandem mass spectra were searched against Mus_musculus_10090_SP_20220107.fasta (17097 entries) concatenated with reverse decoy database. Carbamidomethyl on Cys was specified as a fixed modification, and oxidation of methionine, N-terminal acetylation of protein, and lactylation of lysine were specified as variable modifications. FDR was adjusted to less than 1%.

Transcriptome Principal Component Analysis (PCA)

PCA was performed on the entire transcriptome dataset. Gene filtering: All expressed genes were filtered based on the average read count, with a threshold of average read count > 10 to retain high-confidence expressed genes for subsequent analysis. Data normalization: Variance-stabilized normalization was applied to the filtered gene count data to reduce technical variation and ensure data comparability across samples. PCA execution: The PCA was conducted using the prcomp function integrated in the stats package of R software. This function was used to compute the principal components (PCs) of the normalized transcriptome data. Visualization: The first two

principal components (PC1 and PC2) derived from the PCA were selected for visualization. Scatter plots were generated to map each sample onto the coordinate system defined by PC1 and PC2, with samples from the WT and KO groups labeled separately to illustrate transcriptomic clustering patterns.

Unbiased Identification of Genes Driving Condition-Specific Transcriptomic Differences

Differential expression analysis was re-conducted to screen for genes with significant expression differences between WT and KO groups, using the DESeq2 package in R software. Strict filtering thresholds were set to ensure the reliability of differentially expressed genes (DEGs): Adjusted p-value (padj) < 0.01 (to control for false discovery rate); Absolute log2 fold change (|log2FC|) > 1 (to ensure a minimum magnitude of expression change between groups).

To further prioritize genes that drive the transcriptomic separation of WT and KO groups, a "contribution score" was calculated for each DEG. The score was defined as the product of two metrics: ① Absolute log2 fold change (|log2FC|) of the DEG: Reflects the magnitude of expression difference between WT and KO groups; ② Loading value of the DEG on the first principal component (PC1): Reflects the strength of correlation between the DEG' s expression and the primary source of transcriptomic variance (i.e., the "condition" of WT vs. KO) identified in PCA. Genes were then ranked in descending order based on their calculated contribution scores.

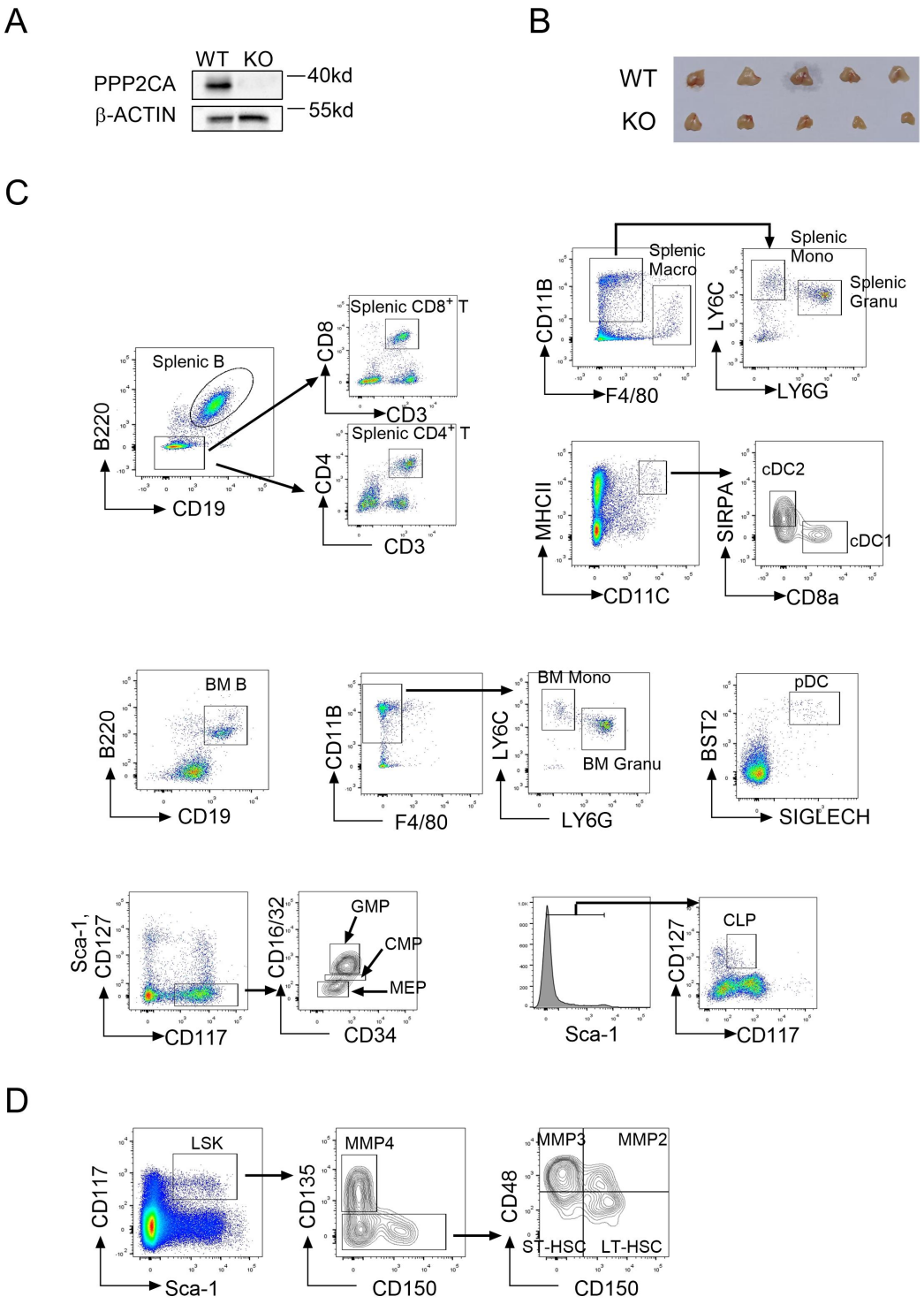

Supplementary Figure 1. The validation of PPP2CA knockout and gating strategies in flow cytometry analysis. (A) Immunoblotting analysis of the KO efficiency of PPP2CA protein in BM Lin$^-$ cells from the tamoxifen pre-treated *Ppp2ca*$^{f/f}$ (WT) and *Ert2*^{cre}*Ppp2ca*$^{f/f}$ (KO) mice. β-ACTIN was used as the internal loading control. Representative data of two repeated experiments. (B) The thymic atrophy observed in *Ppp2ca*-deficient mice. (C) Gating strategies for cell subpopulations. B cells, B220$^+$CD19$^+$; splenic CD4$^+$ T cells, CD19$^-$B220$^-$CD3$^+$CD4$^+$;

splenic $CD8^+$ T cells, $CD19^-B220^-CD3^+CD8^+$; monocytes, $CD11B^+F4/80^-Ly6C^{high}Ly6G^-$; granulocytes, $CD11B^+F4/80^-Ly6C^{low}Ly6G^{high}$; macrophages, $F4/80^+$; pDC, $SIGLECH^+BST2^+$; splenic cDC1, $MHCII^+CD11C^+SIRPA^-CD8\alpha^+$; splenic cDC2, $MHCII^+CD11C^+SIRPA^+CD8\alpha^-$. Lineage cells in BM were removed with lineage cocktail antibodies, and lin^- cells were stained with indicated antibodies. GMP, $Lin^-CD127^-CD117^+Sca\text{-}1^-CD34^+CD16/32^+$; CMP, $Lin^-CD127^-CD117^+Sca\text{-}1^-CD34^+CD16/32^{low/-}$; MEP, $Lin^-CD127^-CD117^+Sca\text{-}1^-CD34^-CD16/32^-$; CLP, $Lin^-CD127^+CD117^{int}Sca\text{-}1^{int}$. (**D**) LSK, $Lin^-CD117^+Scal\text{-}1^+$; LT-HSC, $Lin^-CD117^+Scal\text{-}1^+CD135^-CD150^+CD48^-$; ST-HSC, $Lin^-CD117^+Scal\text{-}1^+CD135^-CD150^-CD48^-$; MPP2, $Lin^-CD117^+Scal\text{-}1^+CD135^-CD150^+CD48^+$; MPP3, $Lin^-CD117^+Scal\text{-}1^+CD135^-CD150^-CD48^+$; MPP4, $Lin^-CD117^+Scal\text{-}1^+CD135^+CD150^-CD48^+$.

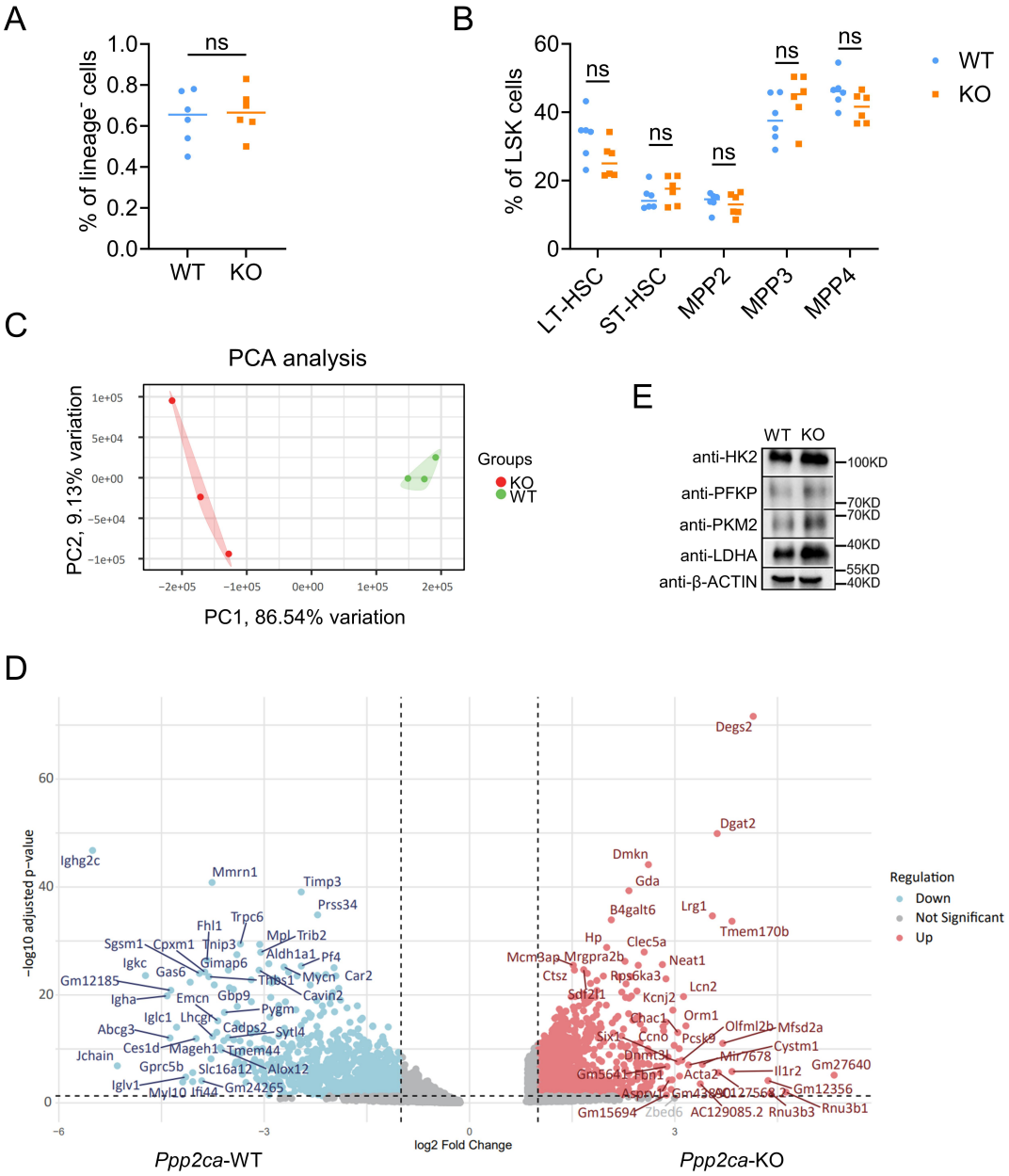

Supplementary Figure 2. (A) The proportion of LSK cells in BM Lin- cells. (B) The proportion of LT-HSC, ST-HSC, MMP2, MMP3 and MMP4 in BM LSK cells. (C) The principal component analysis (PCA) to evaluate global transcriptomic separation between *Ppp2ca*$^{f/f}$ (WT) and *Ert2*^{cre}*Ppp2ca*$^{f/f}$ (KO) LSK cells. (D) A volcano plot was generated to visualize differentially expressed genes (DEGs) between WT and KO LSK cells. The x-axis represents the log2 fold change (log2FC) in gene expression, where positive values indicate upregulation and negative values denote downregulation in KO cells relative to WT cells. The y-axis denotes the -log10 (adjusted p-value [padj]), with higher y-values corresponding to more statistically significant differences in gene expression. (E) WT and KO mice were were treated

with tamoxifen for 5 consecutive days. On day 5 after the last tamoxifen injection, BM LSK cells were isolated from the mice and subjected to immunoblotting analysis to detect the protein levels of HK2, PFKP, PKM2, and LDHA. β-ACTIN was used as the loading control to ensure equal protein loading.

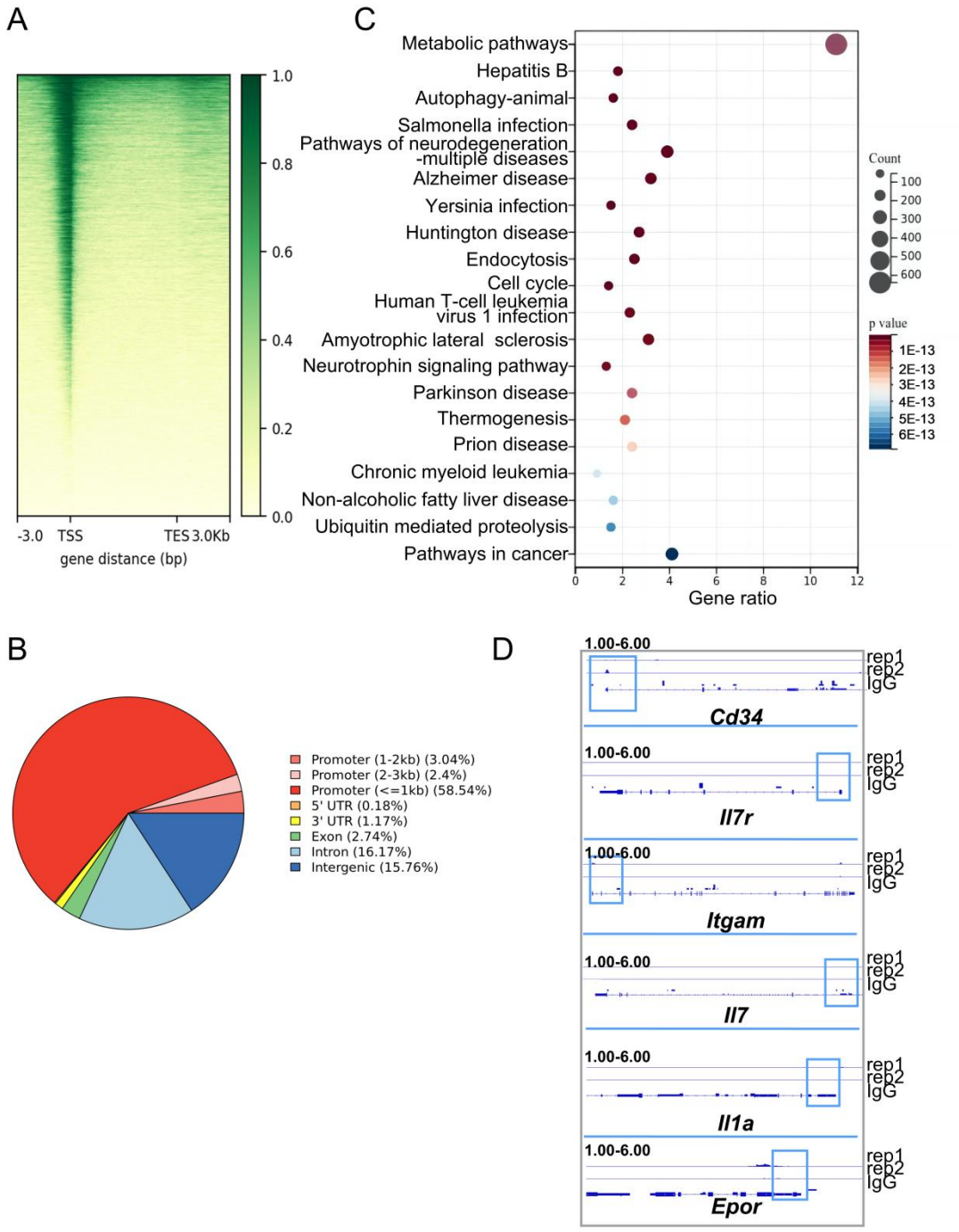

Supplementary Figure 3. *Ppp2ca* keeps the transcription of glycolytic genes in check. (A) Heatmaps depicting the genome-wide occupancy of PPP2CA. Color-scaled intensities depict the genomic occupancy of PPP2CA across all genes, visualized within a 6-kb region extending from 3 kb upstream of the TSS (transcription start site) to 3 kb downstream of the TES (transcription end site). (B) Overview of the genome-wide distribution of PPP2CA binding loci. (C) Enriched pathways of genes with PPP2CA occupancy. (D) The genome browser track depicting PPP2CA signal at representative target genes loci. Blue rectangles highlight the peak regions of PPP2CA enrichment on the promoter target genes. Results from replicate experiments are displayed. rep, repeat.

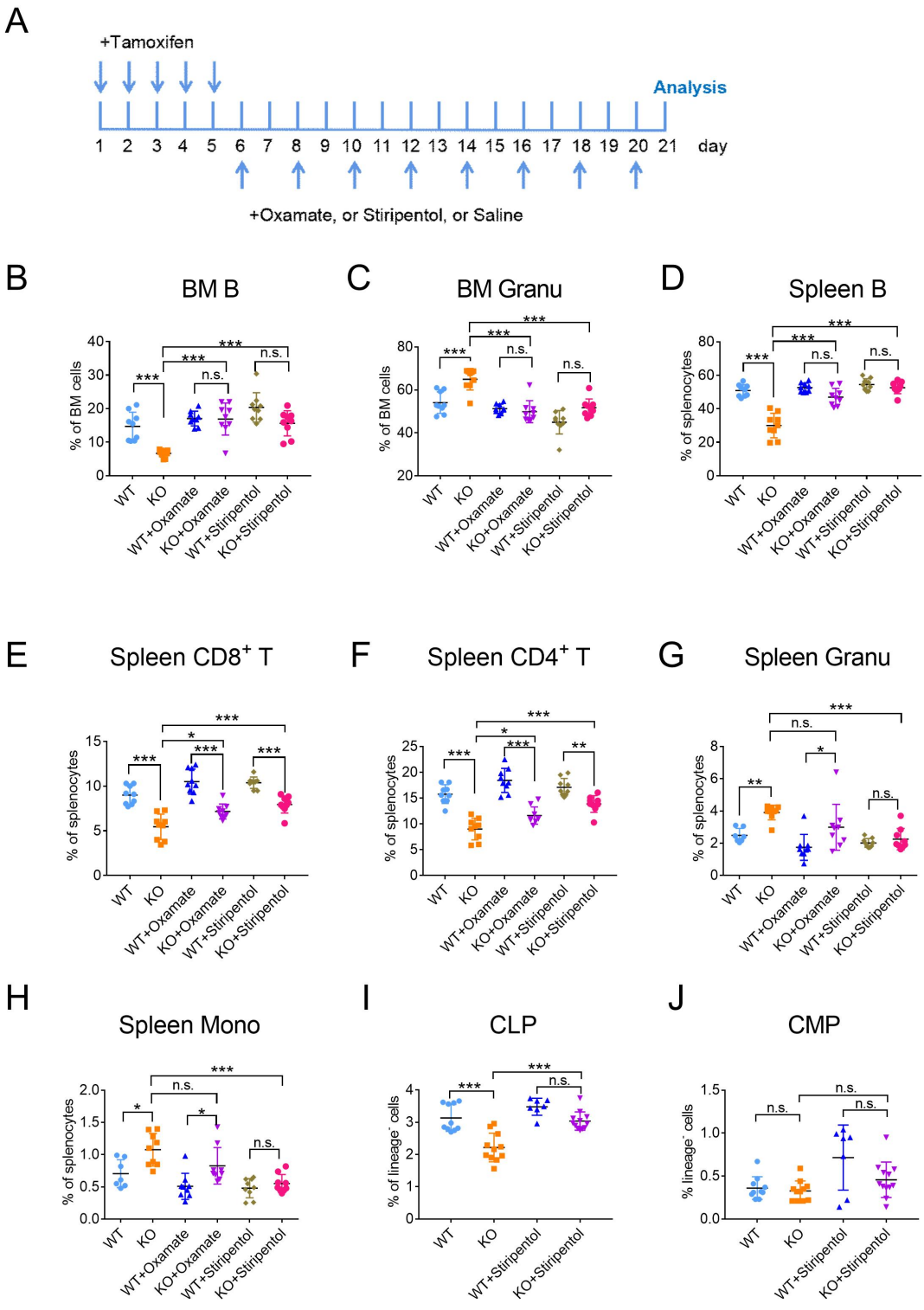

Supplementary Figure 4. Pharmacological interventions targeting lactate metabolism reverse the hematopoietic defects caused by *Ppp2ca* deficiency. (A) Design of the experiments. Tamoxifen pre-treated *Ppp2ca*$^{f/f}$ (WT) and *Ert2*^{cre}*Ppp2ca*$^{f/f}$ (KO) mice were intraperitoneally injected with oxamate, striripentol or saline every other day. (B-J) The proportion of BM B cells (B), BM granulocytes (C), splenic B cells (D), splenic CD8$^+$ T cells (E), splenic CD4$^+$ T cells (F), splenic granulocytes (G),

splenic monocytes (H), BM CLP (I) and BM CMP (J). n=7-12. *p* values were determined by one-way ANOVA. Data are presented as mean ± SEM. (*p<0.05, **p<0.01, ***p<0.001, n.s. not significant).

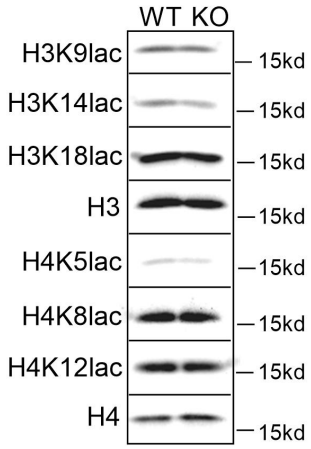

Supplementary Figure 5. Deficiency of *Ppp2ca* exerts no impact on histone lactylation. A screening for differential histone lactylation in Lin$^-$ cells isolated from the BM of tamoxifen treated *Ppp2ca$^{f/f}$* (WT) and *Ert2^{cre}Ppp2ca$^{f/f}$* (KO) mice. The levels of histone lactylation were analyzed by immunoblot.

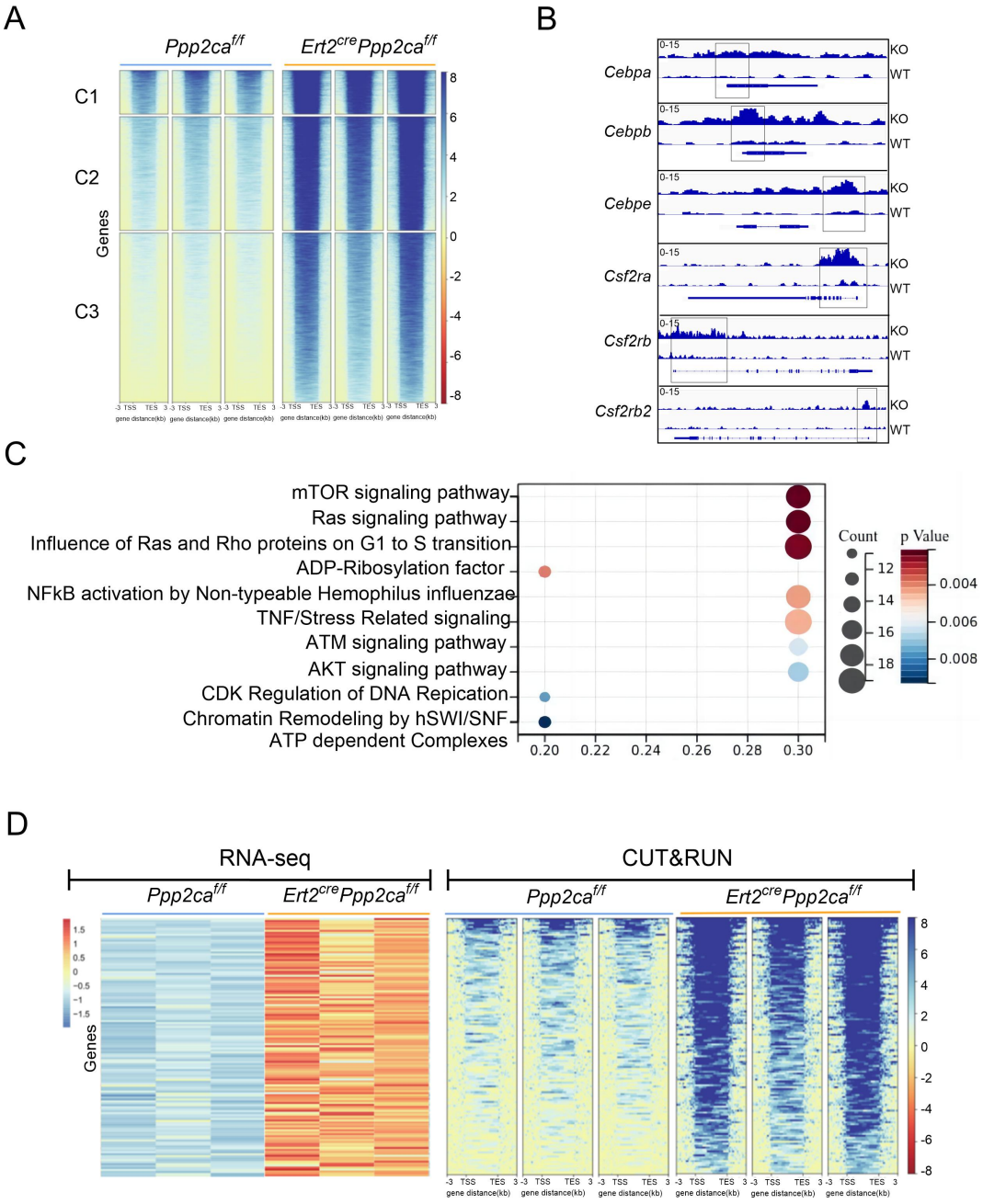

Supplementary Figure 6. *Ppp2ca* deficiency results in elevated acetylation of H3K27. LSK cells were isolated from the BM of tamoxifen treated *Ppp2ca*$^{f/f}$ (WT) and *Ert2*^{cre}*Ppp2ca*$^{f/f}$ (KO) mice. (A) Heatmaps of genome-wide occupancy of H3K27ac in LSK. Color-scaled intensities of all genes at each site within the range of 3kb upstream of the TSS (transcriptional start site) to 3kb downstream of the TES (transcriptional end site) are shown. C1, C2 and C3 indicate gene clusters 1, 2 and 3 with H3K27 acetylation from high to low. (B) The genomic browser track presenting the H3K27ac signal at the loci of representative target genes. The rectangles indicate the peak regions of H3K27ac occupancy on the promoters of target genes. (C) KEGG pathway analysis of genes with elevated H3K27ac modification. (D) Heatmaps depicting the H3K27ac occupancy on genes that were upregulated in the *Ppp2ca*

deficient LSK. The left heatmaps depict the upregulated genes according to the RNA sequencing data in Figure 2, and the right heatmaps illustrate the H3K27ac occupancy on corresponding genes. n=3.

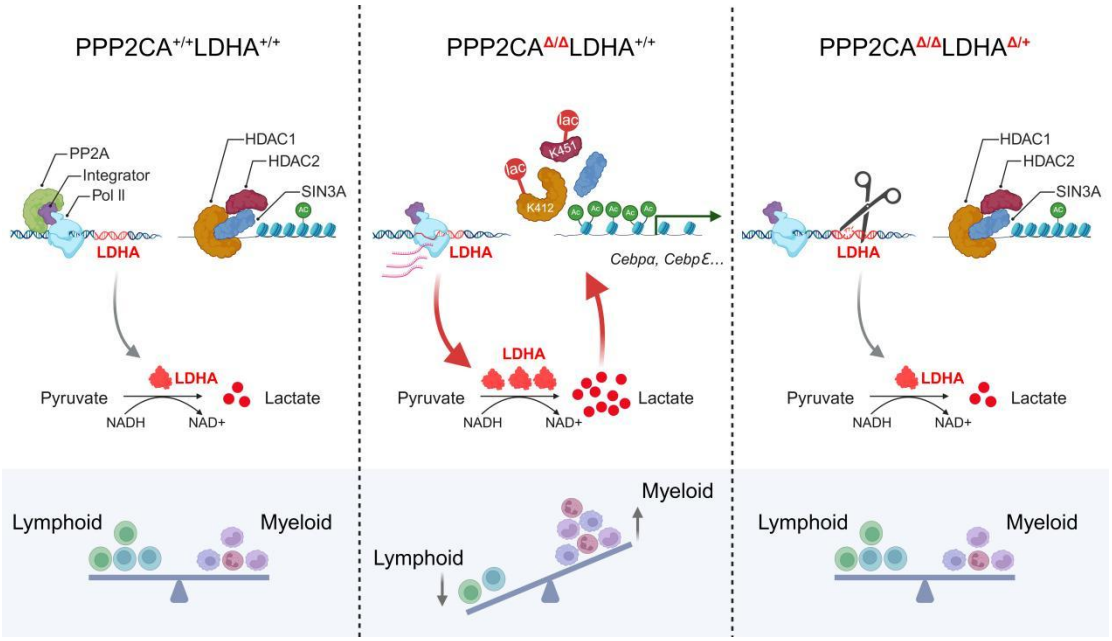

Supplementary Figure 7. Proposed model of this study. *Ppp2ca* deficiency facilitates the RNA Pol II mediated transcriptional initiation of glycolytic genes, including Ldha. Elevated level of lactate leads to lactylation of the 412th lysine (K412) in HDAC1 and the 451st lysine (K451) in HDAC2, impairing the assembly of the HDAC1/2-SIN3A complex on chromatin. Subsequently, the acetylation of histone is enhanced and the expression of myeloid determination genes is upregulated. Consequently, there is an increase in the population of myeloid cells accompanied by a decrease in that of lymphoid cells. Haploid deletion of *Ldha*, the pivotal enzyme responsible for lactate generation, is found to be sufficient to alleviate the myeloid biased differentiation caused by *Ppp2ca* ablation without affecting normal hematopoiesis.

SupplementaryTable 1. List of antibodies and reagents

Antibodies	Source	Cat#
Anti-mouse PDCA1-BV421	BioLegend	127023
Anti-mouse CD4-FITC	BioLegend	100406
Anti-mouse CD34-FITC	BD Bioscience	553733
Anti-mouse B220-PE-CY7	BioLegend	103222
Anti-mouse MHCII-BV510	BioLegend	107636
Anti-mouse CD11c-percpcy5.5	BioLegend	136504
Anti-mouse CD11c-FITC	BioLegend	117306
Anti-mouse CD19-BV510	BioLegend	115546
Anti-mouse Ly-6A/E (Sca-1)-PE-CY7	BioLegend	108114
Anti-mouse CD3-APC	BioLegend	100236
Anti-mouse CD172a-APC	BioLegend	144014
Anti-mouse CD8α-Percp-cy5.5	BioLegend	100736
Anti-mouse SiglecH-PE-CY7	eBioscience	25-0333-82
Anti-mouse CD117-APC	BioLegend	135108
Anti-mouse CD117-PE	BioLegend	135106
Anti-mouse CD127-PE	BioLegend	135010
Anti-mouse CD16/32-APC	BioLegend	101326
Anti-mouse/human CD11b-PE-CY7	BioLegend	101216
Anti-mouse F4/80-PE	BioLegend	123110
Ultra-LEAF™ Purified anti-mouse CD3 Antibody	BioLegend	100238

Ultra-LEAF™ Purified anti-mouse/human CD11b Antibody	BioLegend	101248
Ultra-LEAF™ Purified anti-mouse TER-119 Antibody	BioLegend	116254
Ultra-LEAF ™ Purified anti-mouse/human CD45R/B220 Antibody	BioLegend	103270
Ultra-LEAF™ Purified anti-mouse CD19 Antibody	BioLegend	115570
Ultra-LEAF ™ Purified anti-mouse Ly-6G/Ly-6C (Gr-1) Antibody	BioLegend	108436
Ultra-LEAF™ Purified anti-mouse CD2 Antibody	BioLegend	100119
BioMag Goat anti-Rat IgG (Fc Specific)	Bangs Laboratories	BM548
β-Actin (13E5) Rabbit mAb	Cell Signaling Technology	#4970
Protein G beads	Cell Signaling Technology	#70024
Anti-rabbit IgG, HRP-linked Antibody	Cell Signaling Technology	#7074
Acetyl-Histone H3 (Lys27) (D5E4) XP® Rabbit	Cell Signaling Technology	8173
Histone H3 (D1H2) XP® Rabbit mAb	Cell Signaling Technology	4499
Phospho-Rpb1 CTD (Ser5) (D9N5I) Rabbit mAb	Cell Signaling Technology	13523
PP2A C Subunit Antibody	Cell Signaling	2038

	Technology	
HDAC1 (D5C6U) XP® Rabbit mAb	Cell Signaling Technology	34589
HDAC2 (D6S5P) Rabbit mAb	Cell Signaling Technology	57156
DYKDDDDK Tag (D6W5B) Rabbit mAb	Cell Signaling Technology	14793
PKM2 (D78A4) XP® Rabbit mAb	Cell Signaling Technology	4053
Hexokinase II (C64G5) Rabbit mAb	Cell Signaling Technology	2867
Anti-PFKP 抗体[OTI1D6]	Abcam	ab119796
SIN3A (D1B7) Rabbit mAb	Cell Signaling Technology	7691
Anti-L-Lactyl Lysine Rabbit pAb	PTMBIO	PTM-1401
Lactyl-Histone Antibody Sampler Kit	PTMBIO	PTM-7093
SimpleChIP® Plus Enzymatic Chromatin IP Kit (Magnetic Beads)	Cell Signaling Technology	9005
CellROX™ Green Reagent	ThermoFisher Scientific	C10492
MitoSOX™ Red Reagent	ThermoFisher Scientific	M36008
DCFH-DA	ThermoFisher Scientific	C6827
Red blood cell lysis buffer	ThermoFisher Scientific	00-4333-57

Cell Staining Buffer	BioLegend	420210
Hyperactive Universal CUT&Tag Assay Kit for Illumina	Vazyme	TD903-02
Hyperactive pG-MNase CUT&RUN Assay Kit for Illumina	Vazyme	HD102-01
Pierce™Classic Magnetic IP/Co-IP Kit	ThermoFisher Scientific	88804
SuperBlock™ (TBS) Blocking Buffer	ThermoFisher Scientific	37535
DMEM (Dulbecco's Modified Eagle Medium)	ThermoFisher Scientific	11965092
RPMI 1640 Medium	ThermoFisher Scientific	61870010
Penicillin-Streptomycin	ThermoFisher Scientific	15070063
Fetal Bovine Serum (FBS)	ThermoFisher Scientific	A5670801
BD Horizon™ Fixable Viability Stain 575V	BD Bioscience	565694
L-Lactate Assay Kit (Colorimetric)	Abcam	ab65331
Seahorse XF Glycolytic Rate Assay Kit	Agilent	103344-100
Sodium oxamate	Selleck	S6871
Stiripentol	Selleck	S5266
Tamoxifen	Selleck	S1238
BioMag® Goat anti-Rat IgG	Bangs Labs	BM560
Mouse SCF Recombinant Protein	Peprotech	250-03
Mouse TPO Recombinant Protein	Peprotech	315-14
Mouse FLT3L Recombinant Protein	Peprotech	250-31L
KOD OneTM PCR Master Mix -Blue	TOYOBO	KOD-201
DNase I	Roche	10104159001
Collagenase IV	Sigma-Aldrich	C5138

Supplementary Table 2. Primers used in this study.

Genes	Forward primer (5'-3')	Reverse primer (5'-3')
mouse Ldha	GCCAGCAGTCGCTAGACCTAT	CCAAGTTGTATGACCAGCCCA
mouse Hk2	CTATTTGGCCCCGACTCGC	TGAGCTCCGTGAATAAGCAGG
mouse Pfkp	TTCAGTGCTTGCTGAGTACGG	GCGCTGGAGCTCGAAGAA
mouse Pkm	CTTCAAATCTCCGGGACCCA	GAATGAAGGCAGTCCCTGCT
mouse Atp6v0c	TTCTTCGTTTTTCGGTGTCATGG	TCTAGAGTCCCGCATCGC
mouse Atp5g3	TAAGCCTCTTTTCGCTCCGC	GATCTAGGTGACAGGCGACG
mouse Uqcrfs1	CGAACGAAAGGTCGTCCCTG	GGAAGTGGCCGATAGGACGG
mouse Cd34	CCGGAGCGGTACAGGAGAA	ACTCACGCAGCAGACTCATC
mouse Il7	AGGGCGTGACCCTCTTAATC	CTGAGGAGGCGTCGCTG
mouse Il7r	GCTTAATTCAAGCTGTTTCTGGA	GTTAGAAATGACTCACCATCCTGG
mouse Itgam	GTGCCTGAAATACCACAGTTCAC	CAAGACCCCGCCGACATACC
mouse Cebpa	TTCGATCCGAGACCCGTTTG	CACCCAGTGCCCCAACTG
mouse Cebpb	GCAATGACGCGCACCGA	GGCCGAGCGGGAGGTTTAT
mouse Cebpe	CCTGCCCCTCCCTTAGTCA	CTCCGTCACCAACTCCTACG
mouse Csf2ra	CCCAACCTGCAGATGAGGAA	CTTCCTGCGATGGATGGTGA
mouse Csf2rb	GGGAGGTGGTTATTGCCCTC	CAGCTCTCATGTGCCCTTCA
mouse Csf2rb2	ATGGTGGGGATCGAGCTACT	CAGTGCCCTTTCACAAGCAG